

Energy Minimization in RIS-Assisted UAV-Enabled Wireless Power Transfer Systems

Hong Ren, Zhenkun Zhang, Zhangjie Peng, Li Li, and Cunhua Pan

Abstract—Unmanned aerial vehicle (UAV)-enabled wireless power transfer (WPT) systems offer significant advantages in coverage and deployment flexibility, but suffer from endurance limitations due to the limited onboard energy. This paper proposes to improve the energy efficiency of UAV-enabled WPT systems with multiple ground sensors by utilizing reconfigurable intelligent surface (RIS). Specifically, the total energy consumption of the UAV is minimized, while meeting the energy requirement of each sensor. Firstly, we consider a fly-hover-broadcast (FHB) protocol, in which the UAV radiates radio frequency (RF) signals only at several hovering locations. The energy minimization problem is formulated to jointly optimize the UAV's trajectory, hovering time and the RIS's reflection coefficients. To solve this complex non-convex problem, we propose an efficient algorithm. Specifically, the successive convex approximation (SCA) framework is adopted to jointly optimize the UAV's trajectory and hovering time, in which a minorization-maximization (MM) algorithm that maximizes the minimum charged energy of all sensors is provided to update the reflection coefficients. Then, we investigate the general scenario in which the RF signals are radiated during the flight, aiming to minimize the total energy consumption of the UAV by jointly optimizing the UAV's trajectory, flight time and the RIS's reflection coefficients. By applying the path discretization (PD) protocol, the optimization problem is formulated with a finite number of variables. A high-quality solution for this more challenging problem is obtained. Finally, our simulation results demonstrate the effectiveness of the proposed algorithm and the benefits of RIS in energy saving.

Index Terms—Reconfigurable Intelligent Surface (RIS), unmanned aerial vehicle (UAV), wireless power transfer (WPT), minorization-maximization (MM).

I. INTRODUCTION

WIRELESS power transfer (WPT) enabled by radio frequency (RF) transmission can continuously and

H. Ren and C. Pan are with National Mobile Communications Research Laboratory, Southeast University, Nanjing, China (e-mail: hren@seu.edu.cn; cpan@seu.edu.cn). Z. Zhang and L. Li are with College of Information, Mechanical and Electrical Engineering, Shanghai Normal University, Shanghai, China (e-mail: 1000479070@smail.shnu.edu.cn; lilyxuan@shnu.edu.cn). Z. Peng is with College of Information, Mechanical and Electrical Engineering, Shanghai Normal University, Shanghai, China, and National Mobile Communications Research Laboratory, Southeast University, Nanjing, China, as well as Shanghai Engineering Research Center of Intelligent Education and Bigdata, Shanghai Normal University, Shanghai, China (e-mail: pengzhangjie@shnu.edu.cn). (Corresponding author: Zhangjie Peng and Zhenkun Zhang)

This work was supported in part by the National Key Research and Development Project under Grant 2019YFE0123600, National Natural Science Foundation of China (61701307, 62101128), Basic Research Project of Jiangsu Provincial Department of Science and Technology (BK20210205), High Level Personal Project of Jiangsu Province (JSSCBS20210105), and the open research fund of National Mobile Communications Research Laboratory, Southeast University (2018D14).

Copyright (c) 20xx IEEE. Personal use of this material is permitted. However, permission to use this material for any other purposes must be obtained from the IEEE by sending a request to pubs-permissions@ieee.org.

steadily replenish energy for low-power devices in future Internet-of-things (IoT) networks [1], [2]. Without a wired connection for power supply, IoT devices can be deployed more flexibly and cost less to install, charge and maintain [3]. Nevertheless, traditional WPT systems with fixed energy transmitter are limited in coverage and energy efficiency due to the severe signal attenuation. Dense deployment of energy transmitters may lead to high construction and energy costs.

Unmanned aerial vehicles (UAVs) operating at low altitudes are with high maneuverability and flexibility, and can be dispatched as aerial platforms for data collectors, access points, relays, etc [4], [5]. As a promising solution to improve the quality of wireless communications, the application of UAVs has received extensive attention in recent years. By flying close to the energy devices, UAVs are able to improve the energy harvesting efficiency of WPT systems and wireless powered communication networks (WPCNs) [6]–[8]. In addition, in harsh environments such as forests, mountains, deserts and disaster areas, UAV-enabled WPT can be a more practical and cost-effective solution to extend the lifetime of low-power sensors and IoT devices than terrestrial infrastructures. However, when deploying UAVs in urban areas to track the cars or monitor the dynamic traffic status, the communication link between the UAVs and the ground devices may suffer from the blockages due to the high dense trees, buildings, advertising board, etc. This will result in low energy harvesting efficiency.

As a promising technology for the future wireless communication networks, reconfigurable intelligent surface (RIS) has attracted extensive research attention recently. It improves the quality of wireless communications by reconfiguring the radio propagation environment [9], [10]. With the aid of RISs, the performance of the existing wireless communication systems can be improved significantly [11]–[13]. Furthermore, the integration of RIS into various communication systems has been proposed, for multicell MIMO communications [14], full-duplex cellular communications [15], mobile edge computing [16], and simultaneous wireless information and power transfer (SWIPT) [17]. An RIS is a low-power device with no RF chain, which is a programmable metamaterial planar surface that consists of a large number of passive reflecting elements [18]. Each element independently reflects the incident signal while inducing a digitally controlled phase shift [19]. Thanks to the developments in metamaterials, the phase shifts can be reconfigured in real time [20]. When they are properly adjusted, an RIS can provide substantial passive beamforming gains. Moreover, the signal power at a given receiver can be enhanced by constructively superimposing the reflected and direct signals. It is a cost-efficient solution to

integrate the RIS into UAV-enabled communication systems [21]–[23], and has demonstrated considerable performance enhancement in a variety of scenarios, such as data collection [24], mobile relaying [25] and symbiotic radio systems [26].

Inspired by these advantages, the integration of RIS in UAV communications with WPT has been explored in various scenarios. In [27], the authors proposed a device called the power and data beacon (PDB) to enable the downlink energy and information delivery in systems with a vast number of IoT nodes, and considered the deployment of RIS to assist the information transmission from UAV to PDBs. Based on the technologies of RIS and UAV-mounted cell-free massive MIMO, the authors in [28] proposed a novel framework for time-division energy harvesting of IoT devices. Considering a UAV-enabled WPCN in which IoT devices upload data using the harvested energy with the assistance of RIS, the authors in [29] utilized deep reinforcement learning to maximize the total network rate. In [30], the sum-rate maximization problem was investigated for an RIS-empowered UAV SWIPT scheme, in which a single-antenna UAV simultaneously transmits signals to multiple users, each of which harvests energy with a power splitter. However, as an important challenge hindering the practical application of UAV, the energy consumption has not been considered in the above RIS-assisted WPT scenarios.

In this paper, we consider an RIS-assisted UAV-enabled WPT system, where the UAV is dispatched to provide the required power for multiple ground sensors with minimal energy consumption assisted by an RIS. To maximize the harvested energy, unlike time-division energy transfer scenarios [27], [28], all sensors should always receive the RF signals in our considered scenarios. In this case, it is not optimal to align the phase of the signal transmitted through one UAV-RIS-sensor link with that through the corresponding UAV-sensor direct link. Although the popular semidefinite relaxation (SDR)-based method can be adopted to solve the problems, it has high computational complexity. To address this issue, efficient algorithms are developed for solving the formulated problems. Specifically, we summarize the main contributions of our work as follows:

- 1) To the best of our knowledge, this is the first attempt to explore the benefits of reducing the system energy consumption by deploying an RIS in a UAV-enabled WPT system. Specifically, we consider a WPT system with multiple sensors, and propose to minimize the total energy consumption of the UAV while ensuring sufficient power supply for all sensors. Due to the continuous reception of RF signals by all sensors, the variables in the energy constraints of the energy minimization problems are coupled. Moreover, the complicated non-convex expression of energy consumption and the unit-modulus constraints aggravate the difficulty of solving these problems.
- 2) Under the fly-hover-broadcast (FHB) protocol, we formulate the energy minimization problem for a special scenario and propose an efficient iterative algorithm to solve it. The FHB protocol requires the UAV to visit several hovering locations in sequence and to radiate RF signals only at those locations, which can also serve

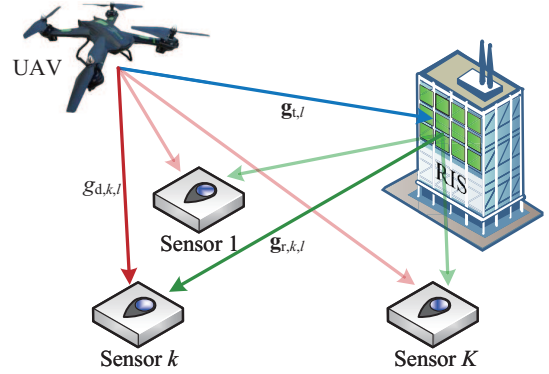


Fig. 1. System model of the RIS-assisted UAV-enabled WPT system.

as the performance lower bound of RIS-assisted UAV-enabled WPT systems. We design an efficient iterative algorithm based on the successive convex approximation (SCA) framework and the minorization-maximization (MM) method. Specifically, in the inner iteration, an MM algorithm is used to optimize the reflection coefficients of the RIS by maximizing the minimum charged energy of all sensors.

- 3) We extend the proposed method to solve the energy minimization problem in the general scenario. Specifically, we apply a *path discretization* (PD) protocol [31] that enables the UAV to radiate RF signals during its flight, and formulate the problem with a finite number of variables. Note that the propulsion energy of UAV accounts for the vast majority of the total energy consumption. The PD protocol brings significant energy saving by reducing the total flight time and providing more freedom for the planning of trajectory and flying speed.
- 4) Simulation results validate the energy efficiency improvement brought by an RIS over traditional UAV-enabled WPT systems, and verify the performance superiority of PD protocol over FHB protocol. Simulation results also validate the performance advantages of the proposed algorithms over the SDR-based benchmark.

The remainder of this paper is organized as follows. Section II describes the system model. In Section III, we formulate the energy minimization problem under the FHB protocol, and develop an efficient algorithm. In Section IV, the proposed method is extended to the general scenario under the PD protocol. Extensive simulation results are shown in Section V. Finally, conclusions are drawn in Section VI.

Notations: Boldface lowercase and uppercase letters respectively denote vectors and matrices. j and \mathbb{C} denote the imaginary unit $\sqrt{-1}$ and the complex field, respectively. The conjugate, transpose, Hermitian and trace of a matrix \mathbf{X} are denoted by \mathbf{X}^* , \mathbf{X}^T , \mathbf{X}^H and $\text{Tr}(\mathbf{X})$, respectively. For a vector \mathbf{x} , $\|\mathbf{x}\|_1$ and $\|\mathbf{x}\|_2$ are its l_1 - and l_2 -norm, respectively. $|x|$, $\text{Re}\{x\}$, $\mathbb{E}\{x\}$ and $\angle(x)$ denote the absolute value, real part, expectation, and angle of a scalar x , respectively.

II. SYSTEM MODEL

Consider a WPT system as shown in Fig. 1, where one rotary-wing UAV with a single transmit antenna is dispatched

TABLE I
NOTATIONS AND TERMINOLOGIES OF PROPULSION POWER

Notation	Physical meaning
P_0	Blade profile power in hovering status
P_i	Induced power in hovering status
U_{tip}	Tip speed of the rotor blade
v_0	Mean rotor induced velocity in hover
d_0	Fuselage drag ratio
ρ	Air density
s	Rotor solidity
A	Rotor disc area

as a mobile power transmitter to serve K ground sensors with the aid of an RIS. The UAV is assumed to fly at a fixed altitude H_U with the maximum speed of V_{max} and a fixed radiated power P_t . Each sensor is equipped with a single receive antenna and a rechargeable battery. The required energy for Sensor k is denoted by E_k^{req} . The positions of all sensors are *a priori* known by the UAV. During each UAV's flight, all sensors continuously charge themselves by harvesting energy from the radiated RF signals, which is enhanced by the RIS. To facilitate the expression in the following discussion, we express the x and y coordinates of the devices by the real and imaginary parts of a complex number, respectively. For instance, the coordinates of Sensor k is denoted by $q_{S,k} = q_{S,k}^x + jq_{S,k}^y$. Additionally, the RIS is deployed at $q_R = q_R^x + jq_R^y$ with altitude H_R .

For a rotary-wing UAV with speed v , the propulsion power can be modeled as [31, Eq. (12)]

$$P_p(v) = P_0 \left(1 + \frac{3v^2}{U_{\text{tip}}^2} \right) + P_i \left(\sqrt{1 + \frac{v^4}{4v_0^4}} - \frac{v^2}{2v_0^2} \right)^{\frac{1}{2}} + \frac{1}{2} d_0 \rho s A v^3. \quad (1)$$

The physical meanings of the parameters in (1) are explained in Table I, and the definitions of which are detailed in the appendix of [31].

For simplicity, we assume that the RIS is equipped with a uniform linear array consisting of M passive reflecting elements. Denote by $\theta_{m,q}$ the phase shift of the m th reflecting element of the RIS when the UAV is at location $q = q^x + jq^y$. The reflection coefficient vector is defined as $\phi_q = [e^{j\theta_{1,q}}, \dots, e^{j\theta_{M,q}}]^T$. The elements in ϕ_q satisfy

$$\theta_{m,q} \in [0, 2\pi), \quad m = 1, \dots, M. \quad (2)$$

When the UAV is at location q , the baseband channels from the UAV to Sensor k , from the UAV to the RIS, and from the RIS to Sensor k are denoted by $g_{d,k,q} \in \mathbb{C}^{1 \times 1}$, $\mathbf{g}_{t,q} \in \mathbb{C}^{M \times 1}$ and $\mathbf{g}_{r,k,q} \in \mathbb{C}^{M \times 1}$, respectively. The Rician fading is assumed for all channels. The channels related to the RIS are modeled as

$$\mathbf{g}_{t,q} = \sqrt{\beta_{t,q}} \left(\sqrt{\frac{\kappa_t}{\kappa_t + 1}} \mathbf{g}_{t,q}^{\text{LoS}} + \sqrt{\frac{1}{\kappa_t + 1}} \mathbf{g}_{t,q}^{\text{NLoS}} \right), \quad (3)$$

$$\mathbf{g}_{r,k,q} = \sqrt{\beta_{r,k}} \left(\sqrt{\frac{\kappa_r}{\kappa_r + 1}} \mathbf{g}_{r,k,q}^{\text{LoS}} + \sqrt{\frac{1}{\kappa_r + 1}} \mathbf{g}_{r,k,q}^{\text{NLoS}} \right), \quad (4)$$

where $\beta_{t,q}$ and $\beta_{r,k}$ represent the large-scale fading coefficients, κ_t and κ_r denote the Rician factors, $\mathbf{g}_{t,q}^{\text{LoS}}$ and $\mathbf{g}_{r,k}^{\text{LoS}}$ denote the deterministic LoS channels, $\mathbf{g}_{t,q}^{\text{NLoS}}$ and $\mathbf{g}_{r,k,q}^{\text{NLoS}}$ are the small-scale channel fading. Each element of $\mathbf{g}_{t,q}^{\text{LoS}}$ and $\mathbf{g}_{r,k,q}^{\text{NLoS}}$ independently follows the circularly symmetric complex Gaussian (CGCS) distribution with zero mean and unit variance. The expressions of $\beta_{t,q}$ and $\beta_{r,k}$ are respectively given by

$$\beta_{t,q} = \frac{\beta_0}{(|q - q_R|^2 + (H_U - H_R)^2)^{\alpha_t/2}} \triangleq \frac{\beta_0}{d_{t,q}^{\alpha_t}}, \quad (5)$$

$$\beta_{r,k} = \frac{\beta_0}{(|q_{S,k} - q_R|^2 + H_R^2)^{\alpha_r/2}} \triangleq \frac{\beta_0}{d_{r,k}^{\alpha_r}}, \quad (6)$$

where β_0 is the channel gain at the reference distance of 1 m, $d_{t,q}$ is the distance between the UAV and the RIS, $d_{r,k}$ is the distance between the RIS and Sensor k , and the corresponding path loss coefficients are denoted by α_t and α_r , respectively. Based on the assumption of uniform linear array, the LoS components of the RIS-related channels $\mathbf{g}_{t,q}^{\text{LoS}}$ and $\mathbf{g}_{r,k}^{\text{LoS}}$ are respectively modeled as

$$\mathbf{g}_{t,q}^{\text{LoS}} = e^{-j\frac{2\pi d_{t,q}}{\lambda}} \left[1, e^{-j\frac{2\pi d}{\lambda} \cos \omega_{t,q}}, \dots, e^{-j\frac{2\pi(M-1)d}{\lambda} \cos \omega_{t,q}} \right]^T, \quad (7)$$

$$\mathbf{g}_{r,k}^{\text{LoS}} = e^{-j\frac{2\pi d_{r,k}}{\lambda}} \left[1, e^{-j\frac{2\pi d}{\lambda} \cos \omega_{r,k}}, \dots, e^{-j\frac{2\pi(M-1)d}{\lambda} \cos \omega_{r,k}} \right]^T, \quad (8)$$

where λ and d denote the wavelength and element spacing of the RIS, respectively, and $\cos \omega_{t,q} = \frac{q_R^x - q^x}{d_{t,q}}$ and $\cos \omega_{r,k} = \frac{q_{S,k}^x - q^x}{d_{r,k}}$ represent the cosine of angle-of-arrival (AoA) and angle-of-departure (AoD), respectively. Similarly, the direct link from the UAV to Sensor k is modeled as

$$g_{d,k,q} = \sqrt{\beta_{d,k,q}} \left(\sqrt{\frac{\kappa_d}{\kappa_d + 1}} g_{d,k,q}^{\text{LoS}} + \sqrt{\frac{1}{\kappa_d + 1}} g_{d,k,q}^{\text{NLoS}} \right), \quad (9)$$

where $\beta_{d,k,q} = \frac{\beta_0}{d_{d,k,q}^{\alpha_d}}$ is the large-scale fading coefficient, $d_{d,k,q} = \sqrt{|q - q_{S,k}|^2 + H_U^2}$ is the distance between the UAV and Sensor k , $g_{d,k,q}^{\text{LoS}} = \exp(-j\frac{2\pi}{\lambda} d_{d,k,q})$ is the LoS channel component, and the NLoS channel component $g_{d,k,q}^{\text{NLoS}}$ follows zero-mean and unit-variance CGCS distribution. Let us introduce a diagonal reflection coefficient matrix $\Phi_q = \text{diag}(\phi_q)$. Then, we can express the equivalent channel spanning from the UAV to Sensor k as $\tilde{g}_{k,q} = g_{d,k,q} + \mathbf{g}_{r,k,q}^H \Phi_q \mathbf{g}_{t,q}$. Accordingly, the received power at Sensor k from the RF signal radiated at location q is given by

$$P_{k,q} = P_t |g_{d,k,q} + \mathbf{g}_{r,k,q}^H \Phi_q \mathbf{g}_{t,q}|^2. \quad (10)$$

Without loss of generality, we assume the same energy conversion efficiency η for all sensors.

Note that in practice, although channel estimation methods for RIS-assisted networks have been proposed in the existing literature [32], it is impossible to estimate the small scale channel fading before the flight. Hence, we design the system based on the long-term channel state information. To this end,

the following theorem provides the expectation of the received power at each sensor $\hat{P}_{k,q} = \mathbb{E}\{P_{k,q}\}$.

Theorem 1. The expected received power $\hat{P}_{k,q}$ at Sensor k is given by

$$\begin{aligned} \hat{P}_{k,q} = & P_t \left(\frac{\kappa_r \kappa_t \beta_{r,k} \beta_{t,q}}{(\kappa_r + 1)(\kappa_t + 1)} \phi_q^H \psi_{k,q} \psi_{k,q}^H \phi_q \right. \\ & + 2\sqrt{\frac{\kappa_d \kappa_r \kappa_t \beta_{d,k,q} \beta_{r,k} \beta_{t,q}}{(\kappa_d + 1)(\kappa_r + 1)(\kappa_t + 1)}} \operatorname{Re}\{\psi_{k,q}^H \phi_q\} \\ & \left. + \beta_{d,k,q} + \frac{M(\kappa_r + \kappa_t + 1)\beta_{r,k}\beta_{t,q}}{(\kappa_r + 1)(\kappa_t + 1)} \right), \end{aligned} \quad (11)$$

where

$$\psi_{k,m,q} \triangleq \frac{2\pi}{\lambda} ((d_{d,k,q} + d_{r,k} - d_{t,q}) + d(\cos \omega_{r,k} - \cos \omega_{t,q})(m-1)), \quad (12)$$

$$\psi_{k,q} \triangleq [e^{-j\psi_{k,1,q}}, \dots, e^{-j\psi_{k,M,q}}]^T. \quad (13)$$

Proof: Please refer to Appendix A. ■

The results in the above theorem will be used in the following sections for the system design.

III. FLY-HOVER-BROADCAST PROTOCOL

The widely adopted FHB protocol is intuitive and easy to implement in practice, which also provides a performance lower bound for the general scenario. In this section, we aim to minimize the total energy consumption of the UAV based on the FHB protocol. An efficient algorithm is developed to solve the formulated problem.

A. Protocol and Energy Consumption Model

Under the FHB protocol, it is assumed that the UAV radiates RF signals only when hovering. The trajectory consists of the initial and final locations q_I and q_F , and $L-1$ hovering locations connected by L straight path segments. We denote the l th hovering location by $q_{U,l} = q_{U,l}^x + jq_{U,l}^y$ for $l \in \mathcal{L}_b$, where $\mathcal{L}_b = \{1, \dots, L-1\}$. On each flight, the UAV starts from q_I , successively visits the hovering locations, and finally arrives at q_F . Then, the total trajectory is denoted by $\mathbf{q}_U = [q_{U,0}, \dots, q_{U,L}]^T \in \mathbb{C}^{(L+1) \times 1}$ with

$$q_{U,0} = q_I, \quad q_{U,L} = q_F. \quad (14)$$

It was derived in [31] that each rotary-wing UAV has a *maximum-range (MR) speed* v_{mr} that maximizes the total travel distance with any given onboard energy, which can be found from the plot of propulsion power $P_p(v)$ versus UAV speed v . With the MR speed v_{mr} , the flight time of the UAV along the l th path segment is given by $\frac{|q_{U,l} - q_{U,l-1}|}{v_{mr}}$. By substituting $v = v_{mr}$ into (1), we have the MR energy consumption $P_p^{mr} = P_p(v_{mr})$. Similarly, the hovering energy consumption is derived as $P_p^{hov} = P_p(0) = P_0 + P_i$. Denoting the hovering time of the UAV at the l th hovering location by t_l , we have the total energy consumption of the UAV as follows

$$E_U^{FHB}(\mathbf{q}_U, \mathbf{t}) = P_p^{mr} \sum_{l=1}^L \frac{|q_{U,l} - q_{U,l-1}|}{v_{mr}} + \sum_{l \in \mathcal{L}_b} (P_p^{hov} + P_t) t_l, \quad (15)$$

where $\mathbf{t} = [t_1, \dots, t_{L-1}]^T$.

B. Problem Formulation

When the UAV is at the l th hovering location, we denote the phase shift of the m th reflecting element of the RIS by $\theta_{m,l}$. $\phi_l = [e^{j\theta_{1,l}}, \dots, e^{j\theta_{M,l}}]^T$ and $\Phi_l = \operatorname{diag}(\phi_l)$ are also defined for $l \in \mathcal{L}_b$, which satisfies

$$\theta_{m,l} \in [0, 2\pi), \quad m = 1, \dots, M, \quad l \in \mathcal{L}_b. \quad (16)$$

Let $\beta_{t,l}$, $\beta_{d,k,l}$ and $\psi_{k,l}$ denote the values of $\beta_{t,q}$, $\beta_{d,k,q}$ and $\psi_{k,q}$ when the UAV is at the l th hovering location, respectively. From (11), the expectation of the received power at Sensor k is given by

$$\begin{aligned} \hat{P}_{k,l} = & P_t \left(\frac{\kappa_r \kappa_t \beta_{r,k} \beta_{t,l}}{(\kappa_r + 1)(\kappa_t + 1)} \phi_l^H \psi_{k,l} \psi_{k,l}^H \phi_l \right. \\ & + 2\sqrt{\frac{\kappa_d \kappa_r \kappa_t \beta_{d,k,l} \beta_{r,k} \beta_{t,l}}{(\kappa_d + 1)(\kappa_r + 1)(\kappa_t + 1)}} \operatorname{Re}\{\psi_{k,l}^H \phi_l\} \\ & \left. + \beta_{d,k,l} + \frac{M(\kappa_r + \kappa_t + 1)\beta_{r,k}\beta_{t,l}}{(\kappa_r + 1)(\kappa_t + 1)} \right). \end{aligned} \quad (17)$$

In this section, we minimize the UAV energy consumption while providing the required energy for all sensors under the FHB protocol, via jointly optimizing the trajectory \mathbf{q}_U , the hovering time \mathbf{t} and the reflection coefficient vectors $\{\phi_l\}$. The energy minimization problem can be formulated as follows

$$\min_{\mathbf{q}_U, \mathbf{t}, \{\phi_l\}} E_U^{FHB}(\mathbf{q}_U, \mathbf{t}) \quad (18a)$$

$$\text{s.t.} \quad t_l \geq 0, \quad l \in \mathcal{L}_b, \quad (18b)$$

$$\eta \sum_{l \in \mathcal{L}_b} t_l \hat{P}_{k,l} \geq E_k^{\text{req}}, \quad k = 1, \dots, K, \quad (18c)$$

$$(14), (16).$$

The main notations used in Problem (18) are summarized in Table II. In Problem (18), the trajectory \mathbf{q}_U , the hovering time \mathbf{t} and the reflection coefficient vectors $\{\phi_l\}$ are jointly optimized. By applying the MR speed v_{mr} , the objective function is transformed to a convex function. However, constraints (16) and (18c) are still non-convex, and all variables are coupled in (18c). In the following, we propose an efficient method for this complicated problem by decoupling it into two subproblems.

C. Optimizing the Trajectory \mathbf{q}_U and Hovering Time \mathbf{t}

In this subsection, we propose an iterative algorithm based on the SCA method to jointly optimize \mathbf{q}_U and \mathbf{t} given $\{\phi_l\}$. From Problem (18), the subproblem of \mathbf{q}_U and \mathbf{t} is formulated as follows

$$\min_{\mathbf{q}_U, \mathbf{t}} E_U^{FHB}(\mathbf{q}_U, \mathbf{t}) \quad (19a)$$

$$\text{s.t.} \quad (14), (18b), (18c).$$

From (17), it can be found that $\hat{P}_{k,l}$ is extremely complex with respect to (w.r.t.) \mathbf{q}_U , which makes the energy requirement constraint (18c) intractable. Fortunately, the change in the value of \mathbf{q}_U per iteration is generally small. Denoting by $\psi_{k,l}^n$ the value of $\psi_{k,l}$ at the n th iteration, the following

TABLE II
MAIN NOTATIONS AND TERMINOLOGIES UNDER FHB PROTOCOL AND PD PROTOCOL

Notation	Definition (FHB protocol)	Definition (PD protocol)
L	Number of hovering locations, $\mathcal{L}_b = \{1, \dots, L-1\}$	Number of path segments, $\mathcal{L}_a = \{1, \dots, L\}$
\mathbf{q}_U	UAV's trajectory, $\mathbf{q}_U = [q_{U,0}, \dots, q_{U,L}]^T$	UAV's trajectory, $\mathbf{q}_U = [q_{U,0}, \dots, q_{U,L}]^T$
\mathbf{t}	UAV's hovering time, $\mathbf{t} = [t_1, \dots, t_{L-1}]^T$	UAV's flight time, $\mathbf{t} = [t_1, \dots, t_L]^T$
$\{\phi_l\}$	RIS's reflection coefficients, $l \in \mathcal{L}_b$	RIS's reflection coefficients, $l \in \mathcal{L}_a$
η	Sensors' energy conversion efficiency	Sensors' energy conversion efficiency
$\hat{P}_{k,l}$	Expected received power at Sensor k , $l \in \mathcal{L}_b$	Expected received power at Sensor k , $l \in \mathcal{L}_a$
E_k^{req}	Required energy for Sensor k	Required energy for Sensor k

approximation can be introduced with limited approximation error

$$\hat{P}_{k,l} \approx P_t \left((U_{1,k,l}^n + U_{3,k,l}) \beta_{t,l} + U_{2,k,l}^n \sqrt{\beta_{d,k,l} \beta_{t,l}} + \beta_{d,k,l} \right), \quad (20)$$

where $U_{1,k,l}^n$, $U_{2,k,l}^n$ and $U_{3,k,l}$ are respectively defined as

$$U_{1,k,l}^n = \frac{\kappa_r \kappa_t \beta_{r,k} \beta_{t,l}}{(\kappa_r + 1)(\kappa_t + 1)} \phi_l^H \psi_{k,l}^n \psi_{k,l}^{n,H} \phi_l, \quad (21)$$

$$U_{2,k,l}^n = 2 \sqrt{\frac{\kappa_d \kappa_r \kappa_t \beta_{d,k,l} \beta_{r,k} \beta_{t,l}}{(\kappa_d + 1)(\kappa_r + 1)(\kappa_t + 1)}} \text{Re} \left\{ \psi_{k,l}^{n,H} \phi_l \right\}, \quad (22)$$

$$U_{3,k,l} = \frac{M(\kappa_r + \kappa_t + 1) \beta_{r,k}}{(\kappa_r + 1)(\kappa_t + 1)}. \quad (23)$$

Then, constraint (18c) is approximated as

$$\frac{\eta}{E_k^{\text{req}}} \sum_{l \in \mathcal{L}_b} P_t t_l \left\{ (U_{1,k,l}^n + U_{3,k,l}) \beta_{t,l} + U_{2,k,l}^n \sqrt{\beta_{d,k,l} \beta_{t,l}} + \beta_{d,k,l} \right\} \geq 1, \quad k = 1, \dots, K. \quad (24)$$

However, constraint (24) is still non-convex. In the following, we utilize the SCA method to transform it to several convex constraints. Firstly, by using the fact that the first-order Taylor expansion is a lower bound of a convex function, we have the following inequalities

$$\beta_{d,k,l} \geq \frac{\beta_0}{\left(|q_{U,l}^n - q_{S,k}|^2 + H_U^2 \right)^{\frac{\alpha_d}{2}}} - \frac{\alpha_d \beta_0 \left(|q_{U,l} - q_{S,k}|^2 - |q_{U,l}^n - q_{S,k}|^2 \right)}{2 \left(|q_{U,l}^n - q_{S,k}|^2 + H_U^2 \right)^{\frac{\alpha_d}{2} + 1}} \triangleq \bar{\beta}_{d,k,l}, \quad (25)$$

$$\beta_{t,l} \geq \frac{\beta_0}{\left(|q_{U,l}^n - q_R|^2 + (H_U - H_R)^2 \right)^{\frac{\alpha_t}{2}}} - \frac{\alpha_t \beta_0 \left(|q_{U,l} - q_R|^2 - |q_{U,l}^n - q_R|^2 \right)}{2 \left(|q_{U,l}^n - q_R|^2 + (H_U - H_R)^2 \right)^{\frac{\alpha_t}{2} + 1}} \triangleq \bar{\beta}_{t,l}, \quad (26)$$

where $q_{U,l}^n$ is the value of $q_{U,l}$ at the n th iteration. Then, the problem to be solved at the n th SCA iteration can be formulated as follows

$$\min_{\mathbf{q}_U, \mathbf{t}, \{y_{t,l}\}, \{y_{d,k,l}\}} E_U^{\text{FHB}}(\mathbf{q}_U, \mathbf{t}) \quad (27a)$$

$$\text{s.t.} \quad \frac{\eta}{E_k^{\text{req}}} \sum_{l \in \mathcal{L}_b} P_t t_l \left((U_{1,k,l}^n + U_{3,k,l}) y_{t,l} + U_{2,k,l}^n \sqrt{y_{t,l} y_{d,k,l}} + y_{d,k,l} \right) \geq 1, \quad k = 1, \dots, K, \quad (27b)$$

$$\bar{\beta}_{t,l} \geq y_{t,l} \geq 0, \quad l \in \mathcal{L}_b, \quad (27c)$$

$$\bar{\beta}_{d,k,l} \geq y_{d,k,l} \geq 0, \quad k = 1, \dots, K, \quad (27d)$$

$$(14), (18b).$$

Note that (27b) is still non-convex, we introduce two sets of slack variables $\{y_{a,k,l}\}$ and $\{e_{k,l}\}$ to transform it as the following constraints

$$(U_{1,k,l}^n + U_{3,k,l}) y_{t,l} + U_{2,k,l}^n y_{a,k,l} + y_{d,k,l} \geq \frac{E_k^{\text{req}} e_{k,l}^2}{\eta P_t t_l}, \quad l \in \mathcal{L}_b, \quad k = 1, \dots, K, \quad (28)$$

$$y_{t,l} \geq \frac{y_{a,k,l}^2}{y_{d,k,l}}, \quad l \in \mathcal{L}_b, \quad k = 1, \dots, K, \quad (29)$$

$$\sum_{l \in \mathcal{L}_b} e_{k,l}^2 \geq 1, \quad k = 1, \dots, K, \quad (30)$$

and utilize the first-order Taylor expansion to transform (30) as

$$\sum_{l \in \mathcal{L}_b} \left(2e_{k,l}^n e_{k,l} - e_{k,l}^{2,n} \right) \geq 1, \quad k = 1, \dots, K, \quad (31)$$

where $e_{k,l}^n$ is the value of $e_{k,l}$ at the n th iteration. Finally, Problem (27) is reformulated as

$$\min_{\mathbf{q}_U, \mathbf{t}, \{y_{t,l}\}, \{y_{d,k,l}\}, \{y_{a,k,l}\}, \{e_{k,l}\}} E_U^{\text{FHB}}(\mathbf{q}_U, \mathbf{t}) \quad (32a)$$

$$\text{s.t.} \quad (14), (18b), (27c), (27d), (28), (29), (31).$$

Problem (32) is a convex problem that can be efficiently solved by the existing optimization tools, such as CVX.

D. Optimizing the Reflection Coefficient Vectors $\{\phi_l\}$

In this subsection, we optimize $\{\phi_l\}$ given \mathbf{q}_U and \mathbf{t} . Note that the objective function of (18) is independent of $\{\phi_l\}$. Hence, the subproblem of $\{\phi_l\}$ is a feasibility-check problem. To improve convergence performance, a common approach is to strengthen the optimization objective to maximize the total oversupplied energy of all sensors [12], [13]. However, due to the energy requirement constraint (18c), the transformed subproblem is not guaranteed to be feasible, which may lead to early convergence of the algorithm. To address this, we set a more challenging optimization objective to maximize the minimum charged energy of all sensors instead. The corresponding subproblem is formulated as follows

$$\max_{\{\phi_l\}, \epsilon} \epsilon \quad (33a)$$

$$\text{s.t.} \quad \frac{\eta}{E_k^{\text{req}}} \sum_{l \in \mathcal{L}_b} t_l \hat{P}_{k,l} \geq \epsilon, \quad k = 1, \dots, K, \quad (33b)$$

$$(16),$$

where ϵ is an auxiliary variable. To guarantee the feasibility, constraint (18c) in Problem (33) is relaxed by removing the constraint $\epsilon \geq 1$. In this paper, we propose to obtain the solution of Problem (18) by solving problems (32) and (33) alternately. Since the former involves the energy requirement constraint (28), the relaxation technique will not change the feasibility of the converged solution in Problem (18). Note that constraint (16) imposes $M(L-1)$ unit-modulus constraints on $\{\phi_l\}$. For schemes with large L , Gaussian randomization in the SDR-based method incurs significant performance loss when solving Problem (33).¹ In the following, we propose a low-complexity algorithm to solve Problem (33) based on the widely used MM method [15], [33]–[35].

To begin with, we reformulate Problem (33) as a more tractable form. By defining

$$\mathbf{A}_{k,l} \triangleq P_t \frac{\kappa_r \kappa_t \beta_{r,k} \beta_{t,l}}{(\kappa_r + 1)(\kappa_t + 1)} \boldsymbol{\psi}_{k,l} \boldsymbol{\psi}_{k,l}^H, \quad (34)$$

$$\mathbf{a}_{k,l} \triangleq P_t \sqrt{\frac{\kappa_d \kappa_r \kappa_t \beta_{d,k,l} \beta_{r,k} \beta_{t,l}}{(\kappa_d + 1)(\kappa_r + 1)(\kappa_t + 1)}} \boldsymbol{\psi}_{k,l}, \quad (35)$$

$$\text{cons}\theta_{k,l} \triangleq P_t \left(\beta_{d,k,l} + \frac{M(\kappa_r + \kappa_t + 1) \beta_{r,k} \beta_{t,l}}{(\kappa_r + 1)(\kappa_t + 1)} \right), \quad (36)$$

we can transform (11) as follows

$$\hat{P}_{k,l} = \phi_l^H \mathbf{A}_{k,l} \phi_l + 2\text{Re} \{ \mathbf{a}_{k,l}^H \phi_l \} + \text{cons}\theta_{k,l}. \quad (37)$$

Then, we define $h_k(\phi) \triangleq \frac{\eta}{E_k^{\text{req}}} \sum_{l \in \mathcal{L}_b} t_l \hat{P}_{k,l}$ and transform it into the following quadratic form

$$\begin{aligned} h_k(\phi) &= \sum_{l \in \mathcal{L}_b} \frac{\eta t_l}{E_k^{\text{req}}} \phi_l^H \mathbf{A}_{k,l} \phi_l + 2 \sum_{l \in \mathcal{L}_b} \frac{\eta t_l}{E_k^{\text{req}}} \text{Re} \{ \mathbf{a}_{k,l}^H \phi_l \} \\ &\quad + \sum_{l \in \mathcal{L}_b} \frac{\eta t_l}{E_k^{\text{req}}} \text{cons}\theta_{k,l} \\ &= \phi^H \mathbf{B}_k \phi + 2\text{Re} \{ \mathbf{b}_k^H \phi \} + \text{cons}\phi_k, \end{aligned} \quad (38)$$

¹Under general protocols, such as the PD protocol applied in Section IV, the value of L is much larger and the performance loss is more severe.

where

$$\boldsymbol{\phi} \triangleq [\phi_1^T, \dots, \phi_{L-1}^T]^T, \quad (39)$$

$$\mathbf{B}_k \triangleq \begin{bmatrix} \frac{\eta t_1}{E_k^{\text{req}}} \mathbf{A}_{k,1} & & \\ & \ddots & \\ & & \frac{\eta t_{L-1}}{E_k^{\text{req}}} \mathbf{A}_{k,L-1} \end{bmatrix}, \quad (40)$$

$$\mathbf{b}_k \triangleq \left[\frac{\eta t_1}{E_k^{\text{req}}} \mathbf{a}_{k,1}^T, \dots, \frac{\eta t_{L-1}}{E_k^{\text{req}}} \mathbf{a}_{k,L-1}^T \right]^T, \quad (41)$$

$$\text{cons}\phi_k \triangleq \sum_{l \in \mathcal{L}_b} \frac{\eta t_l}{E_k^{\text{req}}} \text{cons}\theta_{k,l}. \quad (42)$$

Finally, Problem (33) is reformulated as follows

$$\begin{aligned} \max_{\boldsymbol{\phi}} \quad & \min_k \{ h_k(\boldsymbol{\phi}) \} \\ \text{s.t.} \quad & (16) \end{aligned} \quad (43a)$$

Note that the objective function of Problem (43) is non-differentiable. To address this, we replace it with the following smooth and convex lower bound [36]

$$\min_k \{ h_k(\boldsymbol{\phi}) \} \approx f(\boldsymbol{\phi}) \triangleq -\frac{1}{\mu} \log \left(\sum_{k=1}^K \exp(-\mu h_k(\boldsymbol{\phi})) \right), \quad (44)$$

where $\mu > 0$ is a smoothing parameter. In particular, the following inequalities hold

$$f(\boldsymbol{\phi}) \leq \min_k \{ h_k(\boldsymbol{\phi}) \} \leq f(\boldsymbol{\phi}) + \frac{1}{\mu} \log(K). \quad (45)$$

By replacing the objective function of Problem (43) with $f(\boldsymbol{\phi})$, a convex problem can be obtained. To utilize the MM method, the following theorem provides a tractable minorizing function of $f(\boldsymbol{\phi})$ to formulate the surrogate problem at each iteration.

Theorem 2. Denote by $\boldsymbol{\phi}^r$ the solution at the r th iteration. For any feasible $\boldsymbol{\phi}$, $f(\boldsymbol{\phi})$ is minorized with $\tilde{f}(\boldsymbol{\phi} | \boldsymbol{\phi}^r)$ as follows

$$\tilde{f}(\boldsymbol{\phi} | \boldsymbol{\phi}^r) = 2\text{Re} \{ \mathbf{u}^H \boldsymbol{\phi} \} + \text{cons}\phi_{\text{MM}}. \quad (46)$$

where

$$g_k(\boldsymbol{\phi}^r) \triangleq \frac{\exp(-\mu h_k(\boldsymbol{\phi}^r))}{\sum_{k=1}^K \exp(-\mu h_k(\boldsymbol{\phi}^r))}, \quad (47)$$

$$\mathbf{c} = \sum_{k=1}^K g_k(\boldsymbol{\phi}^r) (\mathbf{B}_k^H \boldsymbol{\phi}^r + \mathbf{b}_k), \quad (48)$$

$$\begin{aligned} \alpha &= -2\mu \max_k \left\{ M \max_l \left\{ \lambda_{\max} \left(\left(\frac{\eta t_l}{E_k^{\text{req}}} \right)^2 \mathbf{A}_{k,l} \mathbf{A}_{k,l}^H \right) \right\} \right. \\ &\quad \left. + \mathbf{b}_k^H \mathbf{b}_k + 2 \|\mathbf{B}_k \mathbf{b}_k\|_1 \right\}, \end{aligned} \quad (49)$$

$$\mathbf{u} \triangleq \mathbf{c} - \alpha \boldsymbol{\phi}^r, \quad (50)$$

$$\text{cons}\phi_{\text{MM}} \triangleq f(\boldsymbol{\phi}^r) - 2\text{Re} \{ \mathbf{c}^H \boldsymbol{\phi}^r \} + 2\alpha M. \quad (51)$$

Proof: Please refer to Appendix B. ■

Algorithm 1 MM algorithm for solving Problem (33)

Initialize: Initial the number of iterations as $r = 1$. Set feasible ϕ^1 , smoothing parameter μ , maximum number of iterations r_{\max} and error tolerance ε_e .

- 1: **repeat**
- 2: Calculate $\hat{\phi}_1 = \mathfrak{M}(\phi^r)$ and $\hat{\phi}_2 = \mathfrak{M}(\hat{\phi}_1)$;
- 3: Calculate $\mathbf{v}_1 = \hat{\phi}_1 - \phi^r$ and $\mathbf{v}_2 = \hat{\phi}_2 - \hat{\phi}_1 - \mathbf{v}_1$;
- 4: Calculate step factor $\sigma = -\frac{\|\mathbf{v}_1\|_2}{\|\mathbf{v}_2\|_2}$;
- 5: Calculate $\phi^{r+1} = \exp(j\angle(\phi^r - 2\sigma\mathbf{v}_1 + \sigma^2\mathbf{v}_2))$;
- 6: If $f(\phi^{r+1}) < f(\phi^r)$, set $\sigma \leftarrow \frac{(\sigma-1)}{2}$ and go to step 2;
- 7: Set $r \leftarrow r + 1$;
- 8: **until** $|f(\phi^{r+1}) - f(\phi^r)| < \varepsilon_e f(\phi^r)$ or $r \geq r_{\max}$;
- 9: If $\min_k \{h_k(\phi^{r+1})\} < \min_k \{h_k(\phi^r)\}$, set $\phi^{r+1} \leftarrow \phi^1$.

By replacing the objective function of Problem (43) with (46), we obtain the surrogate problem at the r th MM iteration

$$\begin{aligned} \max_{\phi} \quad & 2\text{Re}\{\mathbf{u}^H\phi\} + \text{cons}\phi_{\text{MM}} \quad (52a) \\ \text{s.t.} \quad & (16). \end{aligned}$$

It can be readily verified that the optimal solution of Problem (52) is given by

$$\phi^{r+1} = \exp(j\angle\mathbf{u}), \quad (53)$$

where $\exp(\cdot)$ and $\angle(\cdot)$ are element-wise operations.

Based on the above discussions, a modified MM algorithm is proposed to solve Problem (33), the details of which are provided in Algorithm 1, where SQUAREM [37] theory is introduced to accelerate the convergence. Specifically, $\phi^{r+1} = \mathfrak{M}(\phi^r)$ in Step 2 represents the nonlinear fixed-point iteration map given in (53). Thanks to the guaranteed feasibility of Problem (33), ϕ can be efficiently optimized by Algorithm 1 with arbitrary \mathbf{q}_U and \mathbf{t} . Furthermore, the works in [14], [33] and [35] have proved and verified the Karush-Kuhn-Tucker (KKT) optimality of the converged solution of MM algorithm, which indicates that Algorithm 1 can obtain a KKT optimal solution of the relaxed Problem (43) with objective function $f(\phi)$. Moreover, when μ is sufficiently large, the approximation in (44) is tight, and the converged solution is approximately KKT optimal for Problem (33).

E. Algorithm Development

Based on the above discussions, we propose an effective and efficient algorithm for solving Problem (18) in Algorithm 2, named *SCA-MM*. In Step 5 of Algorithm 2, Algorithm 1 is utilized to calculate the optimal ϕ^{n+1} , where ϕ^n in Algorithm 2 is chosen as the initial feasible ϕ^1 of Algorithm 1. In the later stage of Algorithm 2, a large μ is required to improve the approximation accuracy of $f(\phi)$ in (45). On the contrary, a large μ may result in premature convergence to a local stationary point. To take into account both the solution's optimality and the convergence speed, an adjustment factor ι is introduced in Step 6, which gradually increases μ during iterations. Recall that the approximation (20) is introduced

Algorithm 2 SCA-MM algorithm under the FHB protocol

Initialize: Initial the number of iterations as $n = 1$. Set feasible ϕ^1 , \mathbf{q}_U^1 and \mathbf{t}^1 , the maximum number of iterations n_{\max} , and smoothing-related factors μ, μ_{\max} and ι .

- 1: **repeat**
- 2: Given \mathbf{q}_U^n , calculate $U_{1,k,l}^n, U_{2,k,l}^n$ and $U_{3,k,l}^n$ in (21)-(23);
- 3: Set $\{e_{k,l}^n\}$ to hold the equalities in (28);
- 4: Given ϕ^n , calculate the optimal \mathbf{q}_U^{n+1} and \mathbf{t}^{n+1} by solving Problem (32);
- 5: Given \mathbf{q}_U^{n+1} and \mathbf{t}^{n+1} , calculate the optimal ϕ^{n+1} with Algorithm 1;
- 6: Set $\mu \leftarrow \max\{\mu^\iota, \mu_{\max}\}$ and $n \leftarrow n + 1$;
- 7: **until** $n \geq n_{\max}$.

in constraint (28). Hence, the optimal solution to Problem (32) is not guaranteed to satisfy constraint (18c). Although this issue will be addressed when Problem (32) is solved again in a subsequent iteration, Algorithm 2 may not generate monotonically decreasing objective function value of Problem (18). However, the simulations of convergence in Section V show that the fluctuations are not significant.

In the following, we analyze the computational complexity of Algorithm 2, which mainly lies in solving Problem (32) in Step 4 and calculating ϕ^{n+1} in Step 5. Firstly, since Problem (32) involves only linear matrix inequality (LMI) and second-order cone (SOC) constraints, it can be solved by a standard interior point method [38], whose computational complexity is given by

$$\mathcal{O}\left(\sqrt{\underbrace{\sum_{j=1}^J b_j}_{\text{LMI}} + \underbrace{2I}_{\text{SOC}}}\left(\underbrace{n^2 \sum_{j=1}^J b_j^2 + n \sum_{j=1}^J b_j^3}_{\text{LMI}} + \underbrace{n \sum_{i=1}^I a_i^2 + n^3}_{\text{SOC}}\right)\right),$$

where n represents the number of variables, J and I denote the number of LMI and SOC constraints with sizes $\{b_j\}$ and $\{a_i\}$, respectively. Based on the above general expression, the complexity order of solving Problem (32) can be derived as $\mathcal{O}_{S4}^{\text{Alg.2}} = \mathcal{O}(\sqrt{(5K+3)(L-1)} + 2K(n^2K(L-1)^2 + nK(L-1)^3 + n^3))$, where $n = K(L-1)$. Secondly, in each iteration of Algorithm 1, the computational complexity depends on the calculation of α and the values of $h_k(\phi^r)$ for $k = 1, \dots, K$. The corresponding complexity order are given by $\mathcal{O}(K((L-1)^2M^2 + M^3))$ and $\mathcal{O}(K((L-1)^2M^2 + (L-1)M))$, respectively. Denote the number of iterations required for Algorithm 1 to converge by r_{MM} . Then, the complexity of calculating ϕ^{n+1} is of order $\mathcal{O}_{S5}^{\text{Alg.2}} = \mathcal{O}(r_{\text{MM}}K((L-1)^2M^2 + M^3))$. Finally, the overall complexity of Algorithm 2 is given by $\mathcal{O}_{S4}^{\text{Alg.2}} + \mathcal{O}_{S5}^{\text{Alg.2}}$.

IV. PATH DISCRETIZATION PROTOCOL

In order to maximize the harvested energy, the RF signals should be radiated during the UAV's flight, which is not considered in the FHB protocol for simplicity. In this section, the general scenario is studied under the PD protocol. Specifically,

we solve the corresponding problem by extending the proposed method in the previous section.

A. Protocol and Energy Consumption Model

A common method to deal with the continuous flying trajectory of UAV is *time discretization*, where the predetermined duration of entire flight is divided into several time slots. However, this approach is not applicable to our work due to the UAV energy consumption, which is related to the flight time. To address this issue, we adopt the PD method. Specifically, the UAV trajectory is discretized into L path segments that are unequal in length. When the l th path segment is sufficiently short, it can be approximated as the line between its starting point $q_{U,l-1}$ and ending point $q_{U,l}$, where $q_{U,l} = q_{U,l}^x + jq_{U,l}^y$. Then, the total trajectory is denoted by $\mathbf{q}_U = [q_{U,0}, \dots, q_{U,L}]^T \in \mathbb{C}^{(L+1) \times 1}$, where the constraints in (14) still hold.

The following constraints are introduced on the length of path segments $\{\delta_l\}$

$$\delta_l \triangleq |q_{U,l} - q_{U,l-1}| \leq \Delta_{\max}, \quad l \in \mathcal{L}_a, \quad (54)$$

where Δ_{\max} is the maximum length of each path segment and $\mathcal{L}_a = \{1, \dots, L\}$. It is assumed that the UAV flies at a constant speed at each path segment. Due to the high mobility of rotary-wing UAV, the acceleration and deceleration process is ignored. In addition, the value of Δ_{\max} should be chosen appropriately so that the distance from the UAV to each sensor and the RIS is approximately fixed at each path segment. Thus, the coordinates of any point on the l th path segment are regarded as $q_{U,l}$.

Define t_l as the flight time of the UAV along the l th path segment. From (1), the UAV's propulsion power at the l th path segment can be expressed as follows

$$P_{p,l}(t_l) = P_0 \left(1 + \frac{3\delta_l^2}{U_{\text{tip}}^2 t_l^2} \right) + P_1 \left(\sqrt{1 + \frac{\delta_l^4}{4v_0^4 t_l^4}} - \frac{\delta_l^2}{2v_0^2 t_l^2} \right)^{\frac{1}{2}} + \frac{1}{2} d_0 \rho s A \frac{\delta_l^3}{t_l^3}. \quad (55)$$

Then, the total UAV energy consumption of one flight is given by

$$E_U(\mathbf{q}_U, \mathbf{t}) = \sum_{l \in \mathcal{L}_a} t_l (P_t + P_{p,l}(t_l)), \quad (56)$$

where $\mathbf{t} = [t_1, \dots, t_L]^T$.

B. Problem Formulation

Similar to the FHB protocol, when the UAV is at the l th path segment, we denote the phase shift of the m th reflecting element of the RIS by $\theta_{m,l}$, and introduce the definitions $\phi_l = [e^{j\theta_{1,l}}, \dots, e^{j\theta_{M,l}}]^T$ and $\Phi_l = \text{diag}(\phi_l)$ for $l \in \mathcal{L}_a$, which satisfies

$$\theta_{m,l} \in [0, 2\pi), \quad m = 1, \dots, M, \quad l \in \mathcal{L}_a. \quad (57)$$

Additionally, we denote the values of $\beta_{t,q}$, $\beta_{d,k,q}$ and $\psi_{k,q}$ when the UAV is at the l th path segment by $\beta_{t,l}$, $\beta_{d,k,l}$ and $\psi_{k,l}$, respectively. Hence, when the UAV is at the l th path

segment, the expression of the expected received power $\hat{P}_{k,l}$ at Sensor k is the same as (17).

In this section, we propose to provide the required energy for all sensors with minimum energy consumption of the UAV, via jointly optimizing the trajectory \mathbf{q}_U , the flight time \mathbf{t} and the reflection coefficient vectors $\{\phi_l\}$. The energy minimization problem is formulated as follows

$$\min_{\mathbf{q}_U, \mathbf{t}, \{\phi_l\}} E_U(\mathbf{q}_U, \mathbf{t}) \quad (58a)$$

$$\text{s.t.} \quad \delta_l \leq \min\{\Delta_{\max}, V_{\max} t_l\}, \quad l \in \mathcal{L}_a, \quad (58b)$$

$$t_l \geq 0, \quad l \in \mathcal{L}_a, \quad (58c)$$

$$\eta \sum_{l \in \mathcal{L}_a} t_l \hat{P}_{k,l} \geq E_k^{\text{req}}, \quad k = 1, \dots, K, \quad (58d)$$

$$(14), (57).$$

The main notations used in Problem (58) are summarized in Table II. Note that in Problem (58), the objective function $E_U(\mathbf{q}_U, \mathbf{t})$ and the constraints (57) and (58d) are non-convex. Moreover, $E_U(\mathbf{q}_U, \mathbf{t})$ and constraint (58d) are not tractable due to the highly coupled variables. Fortunately, Problem (58) has a similar form to Problem (18). By extending the method in Section III, we propose an efficient algorithm for solving Problem (58) in the following.

C. Optimizing the Trajectory \mathbf{q}_U and Flight Time \mathbf{t}

The proposed method for joint optimization of \mathbf{q}_U and \mathbf{t} under the FHB protocol in Section III-C provides an efficient algorithm framework for the PD protocol. By substituting (55) into (56), we can rewrite $E_U(\mathbf{q}_U, \mathbf{t})$ as follows

$$E_U(\mathbf{q}_U, \mathbf{t}) = \sum_{l \in \mathcal{L}_a} P_t t_l + \sum_{l \in \mathcal{L}_a} P_1 \left(\sqrt{t_l^4 + \frac{\delta_l^4}{4v_0^4}} - \frac{\delta_l^2}{2v_0^2} \right)^{\frac{1}{2}} + \sum_{l \in \mathcal{L}_a} P_0 \left(t_l + \frac{3\delta_l^2}{U_{\text{tip}}^2 t_l} \right) + \frac{1}{2} d_0 \rho s A \sum_{l \in \mathcal{L}_a} \frac{\delta_l^3}{t_l^3}. \quad (59)$$

Then, the subproblem for jointly optimizing the trajectory \mathbf{q}_U and the flight time \mathbf{t} under the PD protocol is formulated as follows

$$\min_{\mathbf{q}_U, \mathbf{t}} E_U(\mathbf{q}_U, \mathbf{t}) \quad (60a)$$

$$\text{s.t.} \quad (14), (58b) - (58d).$$

Compared with the objective function of Problem (19), that of Problem (60) is much more complicated. In the following, we derive a lower bound for $E_U(\mathbf{q}_U, \mathbf{t})$ by applying the SCA method. To begin with, we introduce a set of slack variables $\{x_l \geq 0\}$ and let

$$x_l^2 \geq \sqrt{t_l^4 + \frac{\delta_l^4}{4v_0^4}} - \frac{\delta_l^2}{2v_0^2}, \quad l \in \mathcal{L}_a. \quad (61)$$

It can be derived that

$$\frac{t_l^4}{x_l^2} \leq x_l^2 + \frac{\delta_l^2}{v_0^2}, \quad l \in \mathcal{L}_a. \quad (62)$$

By taking the first-order Taylor expansion of the right hand side of (62) w.r.t. x and δ , we have the following inequality

$$x_l^2 + \frac{\delta_l^2}{v_0^2} \geq 2x_l^n x_l - x_l^{2,n} + \frac{2}{v_0^2} \delta_l^n \delta_l - \frac{1}{v_0^2} \delta_l^{2,n}, \quad l \in \mathcal{L}_a, \quad (63)$$

where x_l^n and δ_l^n are the value of x_l and δ_l at the n th iteration, respectively. Then, to deal with the last term on the right hand side of (59), we introduce three sets of slack variables $\{\delta_l\}$, $\{w_l\}$ and $\{z_l\}$ with

$$\delta_l \leq \bar{\delta}_l, \quad l \in \mathcal{L}_a, \quad (64)$$

$$\frac{\bar{\delta}_l^3}{t_l^2} \leq \frac{z_l^2}{\bar{\delta}_l}, \quad l \in \mathcal{L}_a, \quad (65)$$

$$\frac{z_l^2}{\bar{\delta}_l} \leq w_l, \quad l \in \mathcal{L}_a. \quad (66)$$

Denote by z_l^n the value of z_l at the n th iteration. By utilizing the first-order Taylor expansion, we approximately transform the inequalities in (65) to

$$\frac{\bar{\delta}_l^4}{t_l^2} \leq 2z_l^n z_l - z_l^{2,n}, \quad l \in \mathcal{L}_a. \quad (67)$$

Then, a lower bound for $E_U(\mathbf{q}_U, \mathbf{t})$ is obtained as follows

$$\begin{aligned} \hat{E}_U(\mathbf{q}_U, \mathbf{t}) &= \sum_{l \in \mathcal{L}_a} P_t t_l + \sum_{l \in \mathcal{L}_a} P_i x_l + \sum_{l \in \mathcal{L}_a} P_0 \left(t_l + \frac{3\delta_l^2}{U_{\text{tip}}^2} t_l \right) \\ &+ \frac{1}{2} d_0 \rho s A \sum_{l \in \mathcal{L}_a} w_l. \end{aligned} \quad (68)$$

By replacing $E_U(\mathbf{q}_U, \mathbf{t})$ with $\hat{E}_U(\mathbf{q}_U, \mathbf{t})$, we can formulate the problem at the n th SCA iteration as follows

$$\min_{\substack{\mathbf{q}_U, \mathbf{t}, \{x_l\}, \\ \{\delta_l\}, \{w_l\}, \{z_l\}}} \hat{E}_U(\mathbf{q}_U, \mathbf{t}) \quad (69a)$$

$$\text{s.t.} \quad \frac{t_l^4}{x_l^2} \leq 2x_l^n x_l - x_l^{2,n} + \frac{2}{v_0^2} \delta_l^n \delta_l - \frac{1}{v_0^2} \delta_l^{2,n}, \quad (69b)$$

$$l \in \mathcal{L}_a, \quad (69c)$$

$$(14), (58b) - (58d), (64), (66), (67).$$

Note that in Problem (69), constraint (58d) is still non-convex. We follow the similar strategy as in Section III-C to address this energy constraint. By taking the approximation in (20), we first transform constraint (58d) as follows

$$\begin{aligned} \frac{\eta}{E_k^{\text{req}}} \sum_{l \in \mathcal{L}_a} P_t t_l \left((U_{1,k,l}^n + U_{3,k,l}) \beta_{t,l} + U_{2,k,l}^n \sqrt{\beta_{d,k,l} \beta_{t,l}} \right. \\ \left. + \beta_{d,k,l} \right) \geq 1, \quad k = 1, \dots, K, \end{aligned} \quad (70)$$

where $U_{1,k,l}^n$, $U_{2,k,l}^n$ and $U_{3,k,l}$ at the n th iteration are given in (21)-(23), respectively. In addition, it can be readily verified that the inequalities in (25) and (26) still hold for $\beta_{t,l}$ and $\beta_{d,k,l}$ under the PD protocol. Thus, (70) is replaced with the following constraints

$$\frac{\eta}{E_k^{\text{req}}} \sum_{l \in \mathcal{L}_a} P_t t_l \left((U_{1,k,l}^n + U_{3,k,l}) y_{t,l} + U_{2,k,l}^n \sqrt{y_{t,l} y_{d,k,l}} \right. \\ \left. + y_{d,k,l} \right) \geq 1, \quad k = 1, \dots, K, \quad (71)$$

$$\bar{\beta}_{t,l} \geq y_{t,l} \geq 0, \quad l \in \mathcal{L}_a, \quad (72)$$

$$\bar{\beta}_{d,k,l} \geq y_{d,k,l} \geq 0, \quad k = 1, \dots, K, \quad (73)$$

where $\{y_{t,l}\}$ and $\{y_{d,k,l}\}$ are slack variables. Furthermore, by introducing slack variables $\{y_{a,k,l}\}$ and $\{e_{k,l}\}$, we transform (71) into the following constraints

$$\begin{aligned} (U_{1,k,l}^n + U_{3,k,l}) y_{t,l} + U_{2,k,l}^n y_{a,k,l} + y_{d,k,l} &\geq \frac{E_k^{\text{req}} e_{k,l}^2}{\eta P_t t_l}, \\ l \in \mathcal{L}_a, \quad k = 1, \dots, K, \end{aligned} \quad (74)$$

$$y_{t,l} \geq \frac{y_{a,k,l}^2}{y_{d,k,l}}, \quad l \in \mathcal{L}_a, \quad k = 1, \dots, K, \quad (75)$$

$$\sum_{l \in \mathcal{L}_a} \left(2e_{k,l}^n e_{k,l} - e_{k,l}^{2,n} \right) \geq 1, \quad k = 1, \dots, K, \quad (76)$$

where $e_{k,l}^n$ is the value of $e_{k,l}$ at the n th iteration. In (76), we have used the fact that the first-order Taylor expansion is a lower bound of a convex function. Finally, Problem (69) is reformulated as follows

$$\begin{aligned} \min_{\substack{\mathbf{q}_U, \mathbf{t}, \{x_l\}, \{\delta_l\}, \{w_l\}, \{z_l\}, \\ \{y_{t,l}\}, \{y_{d,k,l}\}, \{y_{a,k,l}\}, \{e_{k,l}\}}} \hat{E}_U(\mathbf{q}_U, \mathbf{t}) \quad (77a) \\ \text{s.t.} \quad (14), (58b), (58c), (64), (66), \\ (67), (69b), (72) - (76). \end{aligned}$$

Problem (77) is a convex problem that can be efficiently solved by the existing optimization tools, such as CVX.

D. Optimizing the Reflection Coefficient Vectors $\{\phi_l\}$

Similar to Section III-D, we take maximizing the minimum charged energy of all sensors as the objective of optimizing $\{\phi_l\}$. The corresponding optimization problem is given by

$$\max_{\{\phi_l\}, \epsilon} \epsilon \quad (78a)$$

$$\text{s.t.} \quad \frac{\eta}{E_k^{\text{req}}} \sum_{l \in \mathcal{L}_a} t_l \hat{P}_{k,l} \geq \epsilon, \quad k = 1, \dots, K, \quad (78b)$$

$$(57).$$

Note that Problem (78) has the same form as Problem (33) except for the value range of l . Therefore, by setting L as the number of path segments and the index of l as \mathcal{L}_a , the proposed Algorithm 1 in Section III-D can be directly applied for solving Problem (78).

E. Algorithm Development

Based on the above discussions, we develop the SCA-MM method for solving Problem (58), which is summarized in Algorithm 3. It can be found that Algorithm 3 follows a similar framework as Algorithm 2, where the optimal ϕ^{n+1} is calculated with Algorithm 1 in Step 5. Compared with the FHB protocol, the PD protocol achieves higher flexibility in trajectory and flight time planning, which further reduces the energy consumption of the UAV.

Similar to Algorithm 2, the computational complexity of Algorithm 3 mainly lies in solving Problem (77) in Step 4 and calculating ϕ^{n+1} in Step 5. Specifically, the complexity order of solving Problem (77) is $\mathcal{O}_{S_4}^{\text{Alg.3}} = \mathcal{O}(\sqrt{5KL} + 2K + 11L(n^2KL^2 + nKL^3 + n^3))$, where $n =$

Algorithm 3 SCA-MM algorithm under the PD protocol

Initialize: Initial the number of iterations as $n = 1$. Set feasible ϕ^1 , \mathbf{q}_U^1 and \mathbf{t}^1 , the maximum number of iterations n_{\max} , and smoothing-related factors μ, μ_{\max} and ι .

- 1: **repeat**
 - 2: Given \mathbf{q}_U^n , calculate $U_{1,k,l}^n$, $U_{2,k,l}^n$ and $U_{3,k,l}^n$ in (21)-(23);
 - 3: Set $\{x_l^n\}$, $\{z_l^n\}$ and $\{e_{k,l}^n\}$ to hold the equalities in (61), (65) and (74), respectively;
 - 4: Given ϕ^n , calculate the optimal \mathbf{q}_U^{n+1} and \mathbf{t}^{n+1} by solving Problem (77);
 - 5: Given \mathbf{q}_U^{n+1} and \mathbf{t}^{n+1} , calculate the optimal ϕ^{n+1} with Algorithm 1;
 - 6: Set $\mu \leftarrow \max\{\mu^\iota, \mu_{\max}\}$ and $n \leftarrow n + 1$;
 - 7: **until** $n \geq n_{\max}$.
-

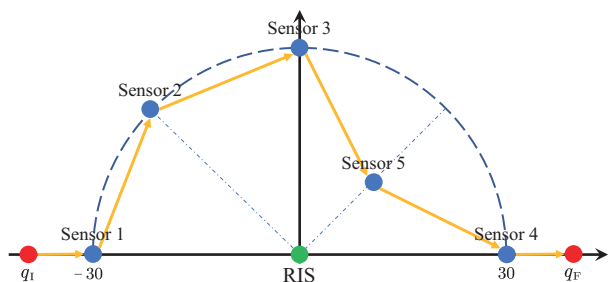


Fig. 2. The simulated RIS-assisted UAV-enabled WPT scenario and the initial trajectory of the UAV.

KL. In addition, the complexity of calculating ϕ^{n+1} is of order $\mathcal{O}_{S5}^{\text{Alg.3}} = \mathcal{O}(r_{\text{MM}}K(L^2M^2 + M^3))$. Hence, the overall complexity of Algorithm 3 is $\mathcal{O}_{S4}^{\text{Alg.3}} + \mathcal{O}_{S5}^{\text{Alg.3}}$.

V. SIMULATION RESULTS

In this section, extensive simulation results are presented to investigate the performance of the RIS-assisted UAV-enabled WPT system with the proposed algorithms.

A. Simulation Setup

Fig. 2 illustrates the simulation scenario, where $K = 5$ sensors are considered to be distributed in a semicircular area with a radius of 30 m. As shown in Fig. 2, the semicircle is divided into four equal parts by five radii, and there is a sensor on each radius. Specifically, Sensor 1-4 are located on the circle, while Sensor 5 is located at the midpoint of the radius. The RIS is deployed at the center of the semicircle with a height of $H_R = 10$ m. The flight height, maximum speed and radiated power of the UAV are set as $H_U = 20$ m, $V_{\max} = 30$ m/s and $P_t = 40$ dBm, respectively. The initial and final locations are $q_I = -35 + j0$ and $q_F = 35 + j0$. The parameters associated with UAV's propulsion power are set to the same as in [31, Table 1], resulting in the MR speed of $v_{\text{mr}} = 18.3$ m/s. Unless otherwise specified, the simulation parameters are set as follows: the energy requirement for each sensor of $E_k^{\text{req}} = E^{\text{req}} = 0.2$ mJ, path loss exponents of $\alpha_t = \alpha_r = 2.2$ and $\alpha_d = 2.6$, Rician factors of $\kappa_t = \kappa_r = \kappa_d = 10$,

$\lambda = 1$ m, $d = 0.5$ m, $\eta = 0.6$, $\Delta_{\max} = 0.5$ m, $\epsilon_e = 10^{-6}$, $r_{\max} = 10$, $\mu = 100$, $\mu_{\max} = 1000$, $\iota = 1.07$, $n_{\max} = 60$.

In the following simulation results, the scheme with Algorithm 2 under the FHB protocol is denoted by **FHB**, and that with Algorithm 3 under the PD protocol is denoted by **PD**. For both protocols, the reflection coefficient vectors $\{\phi_l\}$ are initialized by setting $\theta_{m,l} = 0$, $\forall m, l$. In **FHB**, 5 hovering locations ($L = 6$) are set with the same plane coordinates as the sensors, and the initialized trajectory \mathbf{q}_U is illustrated by the yellow arrows in Fig. 2. In **PD**, the initial value of \mathbf{q}_U is obtained by equally dividing each initialized path segment of **FHB** into portions with length not exceeding $\frac{\Delta_{\max}}{1.8}$ ($L = 362$), and \mathbf{t} is initialized by setting $v_l = v_{\text{mr}}$ for $l \in \mathcal{L}_a$.

B. Convergence of Proposed Algorithms

We first study the convergence of our proposed algorithms. For comparison, the following baseline schemes are also investigated:

- 1) **FHB-SDR**: To analyze the performance of our proposed Algorithm 1, this scheme solves Problem (33) in **PD** by SDR-based method with MOSEK solver [39] and 10^4 Gaussian randomization operations.
- 2) **FHB-noRIS** and **PD-noRIS**: In these two schemes with no RIS deployed, the expected received power is given by $\hat{P}_{k,l}^{\text{noRIS}} = \mathbb{E}\{P_t |g_{d,k,l}|^2\} = P_t \beta_{d,k,l}$. The corresponding energy minimization problems are solved by the methods we propose to solve Problem (19) and (60).
- 3) **FHB-2bit** and **PD-2bit**: Due to hardware limitations, continuously tunable phase shifts are impractical to be implemented on the RIS. To investigate the system performance in practical scenarios, these two schemes with 2 bit resolution are considered, where each element of the optimal phase shifts $\{\theta_{m,l}\}$ obtained by Algorithm 2 and Algorithm 3 is quantized as $0, \frac{\pi}{2}, \pi$ or $\frac{3\pi}{2}$, and \mathbf{q}_U and \mathbf{t} are updated accordingly.

Fig. 3 plots the energy consumption of the UAV versus the number of iterations. It can be observed that **FHB** and **PD** converge in a few iterations. Additionally, thanks to the update strategies in Algorithm 2 and Algorithm 3, there is no obvious fluctuation. These demonstrate the effectiveness of our proposed algorithms in the joint optimization of the UAV's trajectory, flight time and the RIS's reflection coefficients. Moreover, Fig. 3 shows that **FHB** outperforms **FHB-SDR** in both performance and convergence speed, which validates the advantages of Algorithm 1 in the passive beamforming design of the RIS for the entire flight.

C. Energy Saving Performance of RIS

Fig. 4 shows the energy consumption of the UAV versus the number of RIS reflecting elements. Firstly, it is observed that the UAV energy consumption under the PD protocol is significantly lower than that under the FHB protocol. Due to the excellent flexibility in the planning of the UAV's trajectory and flight time, the optimized solutions of PD protocol achieve superior energy saving performance. Secondly, Fig. 4 shows that the energy consumption of the UAV decreases

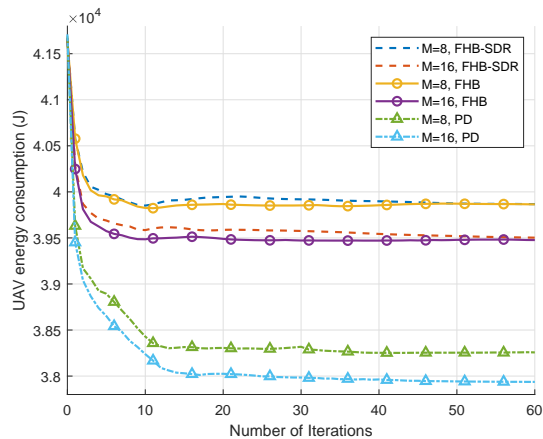


Fig. 3. Convergence of proposed algorithms for $M = [8, 16]$.

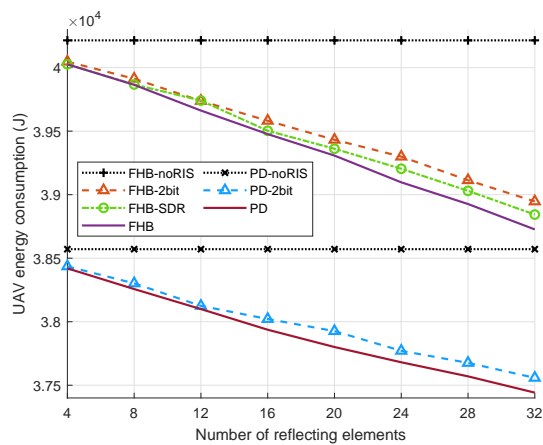


Fig. 4. UAV energy consumption versus the number of RIS reflecting elements.

approximately linearly with the increase of M , which validates the efficiency of RIS on the energy saving. In addition, the performance comparison between **FHB** and **FHB-SDR** again verifies the advantages of Algorithm 1 over SDR-based method. Compared with continuous phase shift schemes, it can also be observed that the performance loss of **2 bit** schemes is slight.

D. Trajectory and Flight Time Planning of UAV

For two cases of the energy requirement $E_k^{\text{req}} = 0.2$ mJ and $E_k^{\text{req}} = 0.02$ mJ, Fig. 5 and Fig. 6 illustrate the optimized UAV's trajectory and flight time, respectively. Firstly, it can be observed from Fig. 5 that for both protocols, the UAV does not fly directly above the sensors. This is as expected since all sensors continually receive RF signals from the UAV and RIS during the flight. Radiating directly above each sensor leads to a longer flight distance, and thus increases the power transmission time. As we mentioned in Section III-A, hovering is not the most energy efficient state for a rotor-wing UAV. Therefore, Fig. 6 shows that under the PD protocol, the UAV maintains a certain speed when it reaches an area favorable for power transmission. Additionally, in the scenario with lower

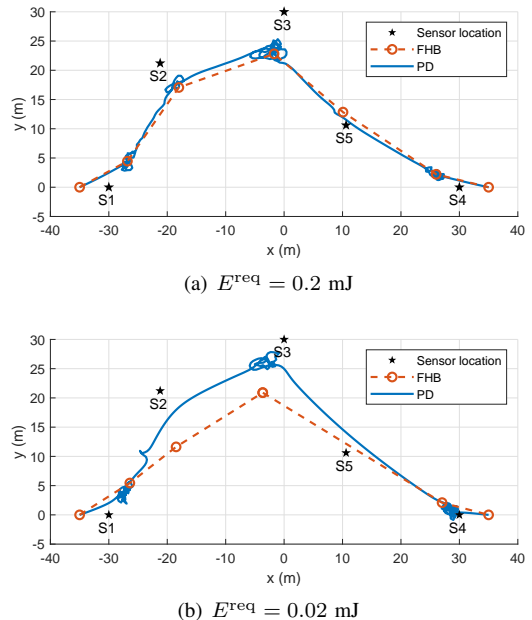


Fig. 5. Optimized UAV's trajectories for different energy requirements of the sensors.

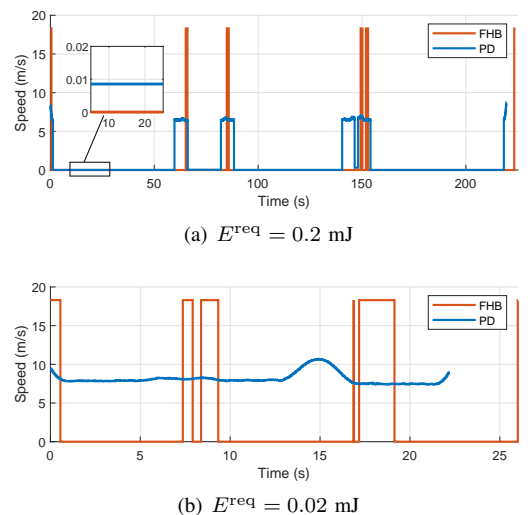


Fig. 6. UAV Speed corresponding to the UAV's trajectories in Fig. 5.

sensor energy requirements, the UAV speed increases as the time required to radiate decreases, as expected.

In Fig. 7, we compare the received power at Sensor 1, 2, 3 and 5. Under the PD protocol, the received power at each sensor is larger than 0 regardless of the UAV's location as expected, which maximizes the harvested energy. Furthermore, by allowing the UAV to radiate RF signals during its flight, the PD protocol enables greater flexibility for the joint design of UAV's trajectory and flight time. From Fig. 5(a) and 5(b), **FHB** tends to reduce both the flight distance and the hovering time as the energy requirements decrease. For the PD protocol, its trend is interesting. From Fig. 7(b), when time duration is from 0 s to 5 s, the received power for Sensor 1 almost keeps stable at its largest value of 4×10^{-6} , which means the UAV may hover over Sensor 1 in this time duration. However, for

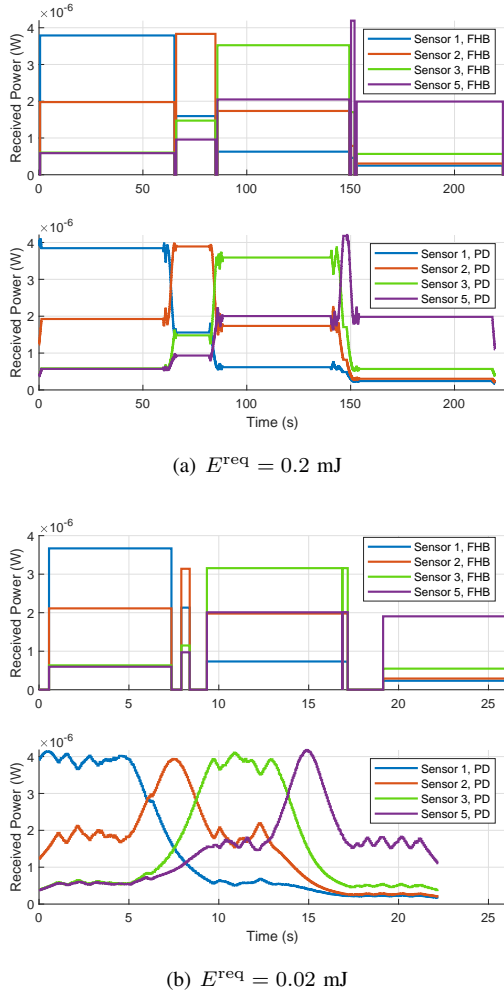


Fig. 7. Received power at Sensor 1, 2, 3 and 5 corresponding to the UAV's trajectories in Fig. 5.

the time duration from 5 s to 10 s, the received power for Sensor 2 firstly increases with the time and then decreases with the time, which implies that the UAV did not hover over Sensor 2. The reason is that Sensor 2 has already harvested enough energy as the UAV keeps transmitting the wireless energy during its flight.

VI. CONCLUSIONS

This paper studied an energy-efficient UAV-enabled WPT system, where the received power of the RF signals at the sensors is enhanced by an RIS. We investigated the problems of providing the required energy for all sensors with minimum UAV energy consumption. Considering the FHB protocol for a simple scenario, the trajectory and hovering time of the UAV and the reflection coefficients of the RIS are jointly optimized. To solve this complex problem, we decoupled the variables by constructing two subproblems. By respectively utilizing the MM method and the SCA framework to solve the subproblems, an efficient iterative algorithm was proposed. For the general scenario, we formulated the energy minimization problem that jointly optimizes the UAV's trajectory, flight time and the RIS's reflection coefficients by applying the PD

protocol. A high-quality solution for this more challenging problem was obtained. Our simulation results demonstrated the effectiveness of the proposed algorithms and the energy saving performance of RIS in UAV-enabled WPT systems.

APPENDIX A PROOF OF THEOREM 1

By substituting (3), (4) and (9) into (10), it can be derived that

$$\begin{aligned} \mathbb{E} \left\{ |g_{d,k,q} + \mathbf{g}_{r,k,q}^H \Phi_q \mathbf{g}_{t,q}|^2 \right\} &= |a_{0,k,q}|^2 + \mathbb{E} \left\{ |a_{1,k,q}|^2 \right\} \\ &+ \mathbb{E} \left\{ |a_{2,k,q}|^2 \right\} + \mathbb{E} \left\{ |a_{3,k,q}|^2 \right\} + \mathbb{E} \left\{ |a_{4,k,q}|^2 \right\}, \end{aligned} \quad (79)$$

where

$$\begin{aligned} a_{0,k,q} &= \sqrt{\frac{\kappa_r \beta_{r,k}}{\kappa_r + 1}} \sqrt{\frac{\kappa_t \beta_{t,q}}{\kappa_t + 1}} (\mathbf{g}_{r,k}^{\text{LoS}})^H \Phi_q \mathbf{g}_{t,q}^{\text{LoS}} \\ &+ \sqrt{\frac{\kappa_d \beta_{d,k,q}}{\kappa_d + 1}} g_{d,k,q}^{\text{LoS}}, \end{aligned} \quad (80a)$$

$$a_{1,k,q} = \sqrt{\frac{\beta_{d,k,q}}{\kappa_d + 1}} g_{d,k,q}^{\text{NLoS}}, \quad (80b)$$

$$a_{2,k,q} = \sqrt{\frac{\beta_{r,k}}{\kappa_r + 1}} \sqrt{\frac{\kappa_t \beta_{t,q}}{\kappa_t + 1}} (\mathbf{g}_{r,k,q}^{\text{NLoS}})^H \Phi_q \mathbf{g}_{t,q}^{\text{LoS}}, \quad (80c)$$

$$a_{3,k,q} = \sqrt{\frac{\kappa_r \beta_{r,k}}{\kappa_r + 1}} \sqrt{\frac{\beta_{t,q}}{\kappa_t + 1}} (\mathbf{g}_{r,k}^{\text{LoS}})^H \Phi_q \mathbf{g}_{t,q}^{\text{NLoS}}, \quad (80d)$$

$$a_{4,k,q} = \sqrt{\frac{\beta_{r,k}}{\kappa_r + 1}} \sqrt{\frac{\beta_{t,q}}{\kappa_t + 1}} (\mathbf{g}_{r,k,q}^{\text{NLoS}})^H \Phi_q \mathbf{g}_{t,q}^{\text{NLoS}}. \quad (80e)$$

It is readily to verify that $\mathbb{E} \left\{ \mathbf{g}_{r,k,q}^{\text{NLoS}} (\mathbf{g}_{r,k,q}^{\text{NLoS}})^H \right\} = \mathbf{I}_M$, $\Phi_q^H \Phi_q = \mathbf{I}_M$ and $(\mathbf{g}_{t,q}^{\text{LoS}})^H \mathbf{g}_{t,q}^{\text{LoS}} = M$. Hence, we have

$$\begin{aligned} &\mathbb{E} \left\{ |a_{2,k,q}|^2 \right\} \\ &= \mathbb{E} \left\{ \frac{\kappa_t \beta_{r,k} \beta_{t,q}}{(\kappa_r + 1)(\kappa_t + 1)} (\mathbf{g}_{t,q}^{\text{LoS}})^H \Phi_q^H \mathbf{g}_{r,k,q}^{\text{NLoS}} (\mathbf{g}_{r,k,q}^{\text{NLoS}})^H \Phi_q \mathbf{g}_{t,q}^{\text{LoS}} \right\} \\ &= \frac{M \kappa_t \beta_{r,k} \beta_{t,q}}{(\kappa_r + 1)(\kappa_t + 1)}. \end{aligned} \quad (81)$$

Similarly, it can be derived that $\mathbb{E} \left\{ |a_{1,k,q}|^2 \right\} = \frac{\beta_{d,k,q}}{\kappa_d + 1}$, $\mathbb{E} \left\{ |a_{3,k,q}|^2 \right\} = \frac{M \kappa_r \beta_{r,k} \beta_{t,q}}{(\kappa_r + 1)(\kappa_t + 1)}$ and $\mathbb{E} \left\{ |a_{4,k,q}|^2 \right\} = \frac{M \beta_{r,k} \beta_{t,q}}{(\kappa_r + 1)(\kappa_t + 1)}$. Let us rewrite $a_{0,k,q}$ as shown in (82) on the top of the next page. Then, with the definitions in (12) and (13), $|a_{0,k,q}|^2$ is derived as shown in (83) on the top of the next page. Finally, the expected received power $\hat{P}_{k,q} = \mathbb{E} \{ P_{k,q} \}$ in (11) can be obtained by using (10) and (79). This thus completes the proof of Theorem 1.

APPENDIX B PROOF OF THEOREM 2

Let $\mathcal{R}_\phi = \{ \phi \mid \theta_{m,l} \in [0, 2\pi), m = 1, \dots, M, l \in \mathcal{L}_b \}$ denote the feasible region of ϕ . Based on the MM method, $f(\phi)$ is said to be minorized with $\tilde{f}(\phi \mid \phi^r)$ if the following conditions are satisfied:

- (L1) $\tilde{f}(\phi \mid \phi^r)$ is continuous w.r.t. ϕ and ϕ^r ;
- (L2) $\tilde{f}(\phi^r \mid \phi^r) = f(\phi^r), \forall \phi^r \in \mathcal{R}_\phi$;
- (L3) $\tilde{f}(\phi \mid \phi^r) \leq f(\phi), \forall \phi, \phi^r \in \mathcal{R}_\phi$;

$$\begin{aligned}
a_{0,k,q} &= \sqrt{\frac{\kappa_r \beta_{r,k}}{\kappa_r + 1}} \sqrt{\frac{\kappa_t \beta_{t,q}}{\kappa_t + 1}} \left(e^{-j \frac{2\pi d_{r,k}}{\lambda}} \left[1, e^{-j \frac{2\pi d}{\lambda} \cos \omega_{r,k}}, \dots, e^{-j \frac{2\pi(M-1)d}{\lambda} \cos \omega_{r,k}} \right]^T \right)^H \begin{bmatrix} e^{j\theta_{1,q}} & & \\ & \ddots & \\ & & e^{j\theta_{M,q}} \end{bmatrix} \\
&\cdot e^{-j \frac{2\pi d_{t,q}}{\lambda}} \left[1, e^{-j \frac{2\pi d}{\lambda} \cos \omega_{t,q}}, \dots, e^{-j \frac{2\pi(M-1)d}{\lambda} \cos \omega_{t,q}} \right]^T + \sqrt{\frac{\kappa_d \beta_{d,k,q}}{\kappa_d + 1}} \exp\left(-j \frac{2\pi d_{d,k,q}}{\lambda}\right) \\
&= \sqrt{\frac{\kappa_r \kappa_t \beta_{r,k} \beta_{t,q}}{(\kappa_r + 1)(\kappa_t + 1)}} \sum_{m=1}^M \exp\left(j \left(\frac{2\pi(d_{r,k} - d_{t,q}) + 2\pi d(\cos \omega_{r,k} - \cos \omega_{t,q})(m-1)}{\lambda} + \theta_{m,q} \right)\right) \\
&\quad + \sqrt{\frac{\kappa_d \beta_{d,k,q}}{\kappa_d + 1}} \exp\left(-j \frac{2\pi d_{d,k,q}}{\lambda}\right) \\
&\triangleq \exp\left(-j \frac{2\pi d_{d,k,q}}{\lambda}\right) \left(\sqrt{\frac{\kappa_d \beta_{d,k,q}}{\kappa_d + 1}} + \sqrt{\frac{\kappa_r \kappa_t \beta_{r,k} \beta_{t,q}}{(\kappa_r + 1)(\kappa_t + 1)}} \sum_{m=1}^M \exp(j(\psi_{k,m,q} + \theta_{m,q})) \right) \quad (82)
\end{aligned}$$

$$\begin{aligned}
|a_{0,k,q}|^2 &= \frac{\kappa_d \beta_{d,k,q}}{\kappa_d + 1} + \frac{\kappa_r \kappa_t \beta_{r,k} \beta_{t,q}}{(\kappa_r + 1)(\kappa_t + 1)} \left| \sum_{m=1}^M \exp(j(\psi_{k,m,q} + \theta_{m,q})) \right|^2 \\
&\quad + 2 \sqrt{\frac{\kappa_d \kappa_r \kappa_t \beta_{d,k,q} \beta_{r,k} \beta_{t,q}}{(\kappa_d + 1)(\kappa_r + 1)(\kappa_t + 1)}} \operatorname{Re} \left\{ \sum_{m=1}^M \exp(j(\psi_{k,m,q} + \theta_{m,q})) \right\} \\
&= \frac{\kappa_r \kappa_t \beta_{r,k} \beta_{t,q}}{(\kappa_r + 1)(\kappa_t + 1)} \phi_q^H \psi_{k,q} \psi_{k,q}^H \phi_q + 2 \sqrt{\frac{\kappa_d \kappa_r \kappa_t \beta_{d,k,q} \beta_{r,k} \beta_{t,q}}{(\kappa_d + 1)(\kappa_r + 1)(\kappa_t + 1)}} \operatorname{Re} \{ \psi_{k,q}^H \phi_q \} + \frac{\kappa_d \beta_{d,k,q}}{\kappa_d + 1} \quad (83)
\end{aligned}$$

(L4) $\tilde{f}'(\phi | \phi^r; \mathbf{d})|_{\phi=\phi^r} = f'(\phi^r; \mathbf{d})$ for $\forall \mathbf{d}$ belonging to the Boulingand tangent cone of \mathcal{R}_ϕ .

Assume that the minorizing function $\tilde{f}(\phi | \phi^r)$ has the following quadratic form

$$\begin{aligned}
\tilde{f}(\phi | \phi^r) &= f(\phi^r) + 2\operatorname{Re} \{ \mathbf{c}^H (\phi - \phi^r) \} \\
&\quad + (\phi - \phi^r)^H \mathbf{C} (\phi - \phi^r), \quad (84)
\end{aligned}$$

where $\mathbf{c} \in \mathbb{C}^{M(L-1) \times 1}$ and $\mathbf{C} \in \mathbb{C}^{M(L-1) \times M(L-1)}$ are undetermined parameters. Then, (L1) and (L2) are always satisfied. In the following, we determine the expressions for \mathbf{c} and \mathbf{C} by (L3) and (L4).

Let ϕ^t be a feasible point in \mathcal{R}_ϕ . Then, the directional derivative of $\tilde{f}(\phi | \phi^r)$ at ϕ^r with direction $(\phi^t - \phi^r)$ is given by

$$2\operatorname{Re} \{ \mathbf{c}^H (\phi^t - \phi^r) \}. \quad (85)$$

While the directional derivative of $f(\phi)$ is

$$2\operatorname{Re} \left\{ \left[\sum_{k=1}^K g_k(\phi^r) (\mathbf{B}_k^H \phi^r + \mathbf{b}_k)^H \right] (\phi^t - \phi^r) \right\}, \quad (86) \quad \text{where}$$

where \mathbf{B}_k , \mathbf{b}_k and $g_k(\phi^r)$ are defined in (40), (41) and (47), respectively. From (L4), the directional derivatives (85) and (86) must be equal. By comparing coefficients, the expression of \mathbf{c} can be identified as follows

$$\mathbf{c} = \sum_{k=1}^K g_k(\phi^r) (\mathbf{B}_k^H \phi^r + \mathbf{b}_k). \quad (87)$$

Denote by $\phi_{m,l}$ the m th element of ϕ_l . In the following, we consider a relaxed condition (L3') by replacing \mathcal{R}_ϕ in (L3) with a relaxed feasible region $\mathcal{R}_\phi^{\text{relax}} \triangleq \{ \phi | |\phi_{m,l}| \leq 1, m=1, \dots, M, l \in \mathcal{L}_b \}$. It will be shown that the conclusion also satisfies (L3). Specifically, we try to identify the expression of \mathbf{C} by setting $\tilde{f}(\phi | \phi^r)$ as the lower bound of $f(\phi)$ for each linear cut in any direction. By introducing an auxiliary variable $\gamma \in [0, 1]$ and letting $\phi = \phi^r + \gamma(\phi^t - \phi^r) \in \mathcal{R}_\phi^{\text{relax}}$, this sufficient condition is formulated as $j(\gamma) \geq J(\gamma)$, where

$$j(\gamma) \triangleq f(\phi^r + \gamma(\phi^t - \phi^r)), \quad (88)$$

$$J(\gamma) \triangleq f(\phi^r) + 2\gamma \operatorname{Re} \{ \mathbf{c}^H (\phi^t - \phi^r) \} + \gamma^2 (\phi^t - \phi^r)^H \mathbf{C} (\phi^t - \phi^r). \quad (89)$$

It can be readily verified that $j(0) = J(0)$. Denote by $\nabla_\gamma j(\gamma)$ the first-order derivative of $j(\gamma)$ w.r.t. γ . It can be derived that

$$\nabla_\gamma j(\gamma) = \sum_{k=1}^K \tilde{g}_k(\gamma) \nabla_\gamma \tilde{h}_k(\gamma), \quad (90)$$

$$\tilde{h}_k(\gamma) \triangleq h_k(\phi^r + \gamma(\phi^t - \phi^r)), \quad (91)$$

$$\tilde{g}_k(\gamma) \triangleq \frac{\exp(-\mu \tilde{h}_k(\gamma))}{\sum_{k=1}^K \exp(-\mu \tilde{h}_k(\gamma))}. \quad (92)$$

By defining $\mathbf{e}_k \triangleq \mathbf{B}_k^H (\gamma(\phi^t - \phi^r) + \phi^r) + \mathbf{b}_k$ and $\tilde{\phi} \triangleq \phi^t - \phi^r$, we have $\nabla_\gamma \tilde{h}_k(\gamma) = 2\operatorname{Re} \{ \mathbf{e}_k^H \tilde{\phi} \}$. It is readily to verify

$$\begin{aligned}
\lambda_{\min}(\mathbf{\Lambda}) &\stackrel{(a1)}{\geq} \sum_{k=1}^K \tilde{g}_k(\gamma) \left(\lambda_{\min} \left(\begin{bmatrix} \mathbf{B}_k & \mathbf{0} \\ \mathbf{0} & \mathbf{B}_k^T \end{bmatrix} \right) - \mu \lambda_{\max} \left(\begin{bmatrix} \mathbf{e}_k \\ \mathbf{e}_k^* \end{bmatrix} \begin{bmatrix} \mathbf{e}_k \\ \mathbf{e}_k^* \end{bmatrix}^H \right) \right) + \mu \lambda_{\min} \left(\begin{bmatrix} \sum_{k=1}^K \tilde{g}_k(\gamma) \mathbf{e}_k \\ \sum_{k=1}^K \tilde{g}_k(\gamma) \mathbf{e}_k^* \end{bmatrix} \begin{bmatrix} \sum_{k=1}^K \tilde{g}_k(\gamma) \mathbf{e}_k \\ \sum_{k=1}^K \tilde{g}_k(\gamma) \mathbf{e}_k^* \end{bmatrix}^H \right) \\
&\stackrel{(a2)}{=} -2\mu \sum_{k=1}^K \tilde{g}_k(\gamma) \mathbf{e}_k^H \mathbf{e}_k \stackrel{(a3)}{\geq} -2\mu \max_k \{ \mathbf{e}_k^H \mathbf{e}_k \}
\end{aligned} \tag{98}$$

$$\begin{aligned}
\mathbf{e}_k^H \mathbf{e}_k &= \|\mathbf{B}_k^H (\gamma (\phi^t - \phi^r) + \phi^r)\|_2^2 + \mathbf{b}_k^H \mathbf{b}_k + 2\text{Re} \{ \mathbf{b}_k^H \mathbf{B}_k^H (\gamma (\phi^t - \phi^r) + \phi^r) \} \\
&\stackrel{(a4)}{\leq} \lambda_{\max}(\mathbf{B}_k^H \mathbf{B}_k) \|\gamma (\phi^t - \phi^r) + \phi^r\|_2^2 + \mathbf{b}_k^H \mathbf{b}_k + 2\text{Re} \{ \mathbf{b}_k^H \mathbf{B}_k^H (\gamma (\phi^t - \phi^r) + \phi^r) \} \\
&\leq M \lambda_{\max}(\mathbf{B}_k^H \mathbf{B}_k) + \mathbf{b}_k^H \mathbf{b}_k + 2\text{Re} \{ \mathbf{b}_k^H \mathbf{B}_k^H (\gamma (\phi^t - \phi^r) + \phi^r) \} \\
&\stackrel{(a5)}{\leq} M \max_l \left\{ \lambda_{\max} \left(\left(\frac{\eta t_l}{E_k^{\text{req}}} \right)^2 \mathbf{A}_{k,l}^H \mathbf{A}_{k,l} \right) \right\} + \mathbf{b}_k^H \mathbf{b}_k + 2 \|\mathbf{B}_k \mathbf{b}_k\|_1
\end{aligned} \tag{100}$$

that $\nabla_{\gamma} j(0) = \nabla_{\gamma} J(0)$. Therefore, a sufficient condition for $j(\gamma) \geq J(\gamma)$ is

$$\nabla_{\gamma}^2 j(\gamma) \geq \nabla_{\gamma}^2 J(\gamma), \quad \forall \gamma \in [0, 1]. \tag{93}$$

The second-order derivative of $\tilde{h}_k(\gamma)$ is given by $\nabla_{\gamma}^2 \tilde{h}_k(\gamma) = 2\tilde{\phi}^H \mathbf{B}_k \tilde{\phi}$. Then, we have

$$\begin{aligned}
\nabla_{\gamma}^2 j(\gamma) &= \sum_{k=1}^K \left(\tilde{g}_k(\gamma) \nabla_{\gamma}^2 \tilde{h}_k(\gamma) - \mu \tilde{g}_k(\gamma) \left(\nabla_{\gamma} \tilde{h}_k(\gamma) \right)^2 \right) \\
&\quad + \mu \left(\sum_{k=1}^K \tilde{g}_k(\gamma) \nabla_{\gamma} \tilde{h}_k(\gamma) \right)^2 \\
&= [\tilde{\phi}^H \quad \tilde{\phi}^T] \mathbf{\Lambda} \begin{bmatrix} \tilde{\phi} \\ \tilde{\phi}^* \end{bmatrix},
\end{aligned} \tag{94}$$

where

$$\begin{aligned}
\mathbf{\Lambda} &= \sum_{k=1}^K \tilde{g}_k(\gamma) \left(\begin{bmatrix} \mathbf{B}_k & \mathbf{0} \\ \mathbf{0} & \mathbf{B}_k^T \end{bmatrix} - \mu \begin{bmatrix} \mathbf{e}_k \\ \mathbf{e}_k^* \end{bmatrix} \begin{bmatrix} \mathbf{e}_k \\ \mathbf{e}_k^* \end{bmatrix}^H \right) \\
&\quad + \mu \begin{bmatrix} \sum_{k=1}^K \tilde{g}_k(\gamma) \mathbf{e}_k \\ \sum_{k=1}^K \tilde{g}_k(\gamma) \mathbf{e}_k^* \end{bmatrix} \begin{bmatrix} \sum_{k=1}^K \tilde{g}_k(\gamma) \mathbf{e}_k \\ \sum_{k=1}^K \tilde{g}_k(\gamma) \mathbf{e}_k^* \end{bmatrix}^H.
\end{aligned} \tag{95}$$

In addition, the second-order derivative of $J(\gamma)$ can be derived as

$$\nabla_{\gamma}^2 J(\gamma) = 2\tilde{\phi}^H \mathbf{C} \tilde{\phi} = [\tilde{\phi}^H \quad \tilde{\phi}^T] \begin{bmatrix} \mathbf{C} & \mathbf{0} \\ \mathbf{0} & \mathbf{C}^T \end{bmatrix} \begin{bmatrix} \tilde{\phi} \\ \tilde{\phi}^* \end{bmatrix}. \tag{96}$$

From (94) and (96), we have $\mathbf{\Lambda} \succeq \begin{bmatrix} \mathbf{C} & \mathbf{0} \\ \mathbf{0} & \mathbf{C}^T \end{bmatrix}$.

Let us define a set of auxiliary matrices $\{\dot{\mathbf{B}}_{k,l}\}$ that satisfies $\mathbf{B}_k = \sum_{l \in \mathcal{L}_b} \dot{\mathbf{B}}_{k,l}$ as follows

$$\dot{\mathbf{B}}_{k,l} = \begin{bmatrix} \mathbf{0}_{(l-1)M} & & \\ & \mathbf{A}_{k,l} & \\ & & \mathbf{0}_{(L-l-1)M} \end{bmatrix}. \tag{97}$$

It can be readily verified that $\text{rank}(\dot{\mathbf{B}}_{k,l}) = \text{rank}(\mathbf{A}_{k,l}) = 1$. Therefore, we have $\text{rank}(\mathbf{B}_k) \leq \sum_{l \in \mathcal{L}_b} \text{rank}(\dot{\mathbf{B}}_{k,l}) = L - 1$

[40, Eq. (1.6.4)]. Similarly, it can be proved that $\begin{bmatrix} \mathbf{B}_k & \mathbf{0} \\ \mathbf{0} & \mathbf{B}_k^T \end{bmatrix}$ is low rank, thus $\lambda_{\min} \left(\begin{bmatrix} \mathbf{B}_k & \mathbf{0} \\ \mathbf{0} & \mathbf{B}_k^T \end{bmatrix} \right) = 0$. To reduce the computational complexity of calculating \mathbf{C} , we set $\mathbf{C} = \alpha \mathbf{I}$, where α is a simple lower bound of $\lambda_{\min}(\mathbf{\Lambda})$. To derive the expression of α , we first obtain the inequalities in (98) on the top of this page with the following lemmas:

- (a1) $\lambda_{\min}(\mathbf{A}) + \lambda_{\min}(\mathbf{B}) \leq \lambda_{\min}(\mathbf{A} + \mathbf{B})$, if \mathbf{A} and \mathbf{B} are Hermitian matrices [41];
- (a2) $\lambda_{\max}(\mathbf{A}) = \text{Tr}(\mathbf{A})$ and $\lambda_{\min}(\mathbf{A}) = 0$, if \mathbf{A} is rank one [41];
- (a3) $\sum_{m=1}^M a_m b_m \leq \max_{m=1}^M \{b_m\}$, if $a_m, b_m \geq 0$ and $\sum_{m=1}^M a_m = 1$ [42, Theorem 30];
- (a4) $\text{Tr}[\mathbf{A}\mathbf{B}] \leq \lambda_{\max}(\mathbf{A}) \text{Tr}[\mathbf{B}]$, if \mathbf{A} is positive semidefinite with maximum eigenvalue $\lambda_{\max}(\mathbf{A})$ and \mathbf{B} is positive semidefinite [41];

In addition, it is readily to verify that

- (a5) $\left[\frac{[\mathbf{B}_k \mathbf{b}_k]_1}{[\mathbf{B}_k \mathbf{b}_k]_1}, \dots, \frac{[\mathbf{B}_k \mathbf{b}_k]_{ML}}{[\mathbf{B}_k \mathbf{b}_k]_{ML}} \right]^T$ and $2 \|\mathbf{B}_k \mathbf{b}_k\|_1$ are the optimal solution and optimal value of the following problem for $\mathbf{x} = [x_1, \dots, x_{ML}]^T$, respectively:

$$\begin{aligned}
\max_{\mathbf{x}} \quad & 2\text{Re} \{ \mathbf{b}_k^H \mathbf{B}_k^H \mathbf{x} \} \\
\text{s.t.} \quad & |x_{ml}| \leq 1, \quad \forall m = 1, \dots, M, l = 1, \dots, L - 1.
\end{aligned} \tag{99a}$$

$$\tag{99b}$$

Recall that $\mathbf{e}_k \triangleq \mathbf{B}_k^H (\gamma (\phi^t - \phi^r) + \phi^r) + \mathbf{b}_k$. The term $\mathbf{e}_k^H \mathbf{e}_k$ can be transformed as shown in (100) on the top of this page. By substituting (100) into (98), the expression of α in (49) is obtained. From (a5), it can be found that $\phi^r + \gamma (\phi^t - \phi^r) \in \mathcal{R}_{\phi}$ when the last equality in (100) holds. In addition, the expression for α is independent of γ . Hence, the proof is completed.

REFERENCES

- [1] C. R. Valenta and G. D. Durgin, "Harvesting wireless power: Survey of energy-harvester conversion efficiency in far-field, wireless power transfer systems," *IEEE Microw. Mag.*, vol. 15, no. 4, pp. 108–120, Jun. 2014.
- [2] Y. Zeng, B. Clerckx, and R. Zhang, "Communications and signals design for wireless power transmission," *IEEE Trans. Commun.*, vol. 65, no. 5, pp. 2264–2290, May 2017.
- [3] D. Niyato, D. I. Kim, M. Maso, and Z. Han, "Wireless powered communication networks: Research directions and technological approaches," *IEEE Wirel. Commun.*, vol. 24, no. 6, pp. 88–97, Dec. 2017.
- [4] M. Mozaffari, W. Saad, M. Bennis, Y.-H. Nam, and M. Debbah, "A tutorial on UAVs for wireless networks: Applications, challenges, and open problems," *IEEE Commun. Surveys Tuts.*, vol. 21, no. 3, pp. 2334–2360, 3rd Quart. 2019.
- [5] Y. Zeng, Q. Wu, and R. Zhang, "Accessing from the sky: A tutorial on UAV communications for 5G and beyond," *Proc. IEEE*, vol. 107, no. 12, pp. 2327–2375, Dec. 2019.
- [6] X. Yuan, T. Yang, Y. Hu, J. Xu, and A. Schmeink, "Trajectory design for UAV-enabled multiuser wireless power transfer with nonlinear energy harvesting," *IEEE Trans. Wireless Commun.*, vol. 20, no. 2, pp. 1105–1121, Feb. 2021.
- [7] L. Xie, J. Xu, and Y. Zeng, "Common throughput maximization for UAV-enabled interference channel with wireless powered communications," *IEEE Trans. Commun.*, vol. 68, no. 5, pp. 3197–3212, May 2020.
- [8] W. Luo, Y. Shen, B. Yang, S. Wang, and X. Guan, "Joint 3-D trajectory and resource optimization in multi-UAV-enabled IoT networks with wireless power transfer," *IEEE Internet Things J.*, vol. 8, no. 10, pp. 7833–7848, May 2021.
- [9] M. Di Renzo, A. Zappone, M. Debbah, M. S. Alouini, C. Yuen, J. de Rosny, and S. Tretyakov, "Smart radio environments empowered by reconfigurable intelligent surfaces: How it works, state of research, and the road ahead," *IEEE J. Sel. Areas Commun.*, vol. 38, no. 11, pp. 2450–2525, Nov. 2020.
- [10] Q. Wu and R. Zhang, "Towards smart and reconfigurable environment: Intelligent reflecting surface aided wireless network," *IEEE Commun. Mag.*, vol. 58, no. 1, pp. 106–112, Jan. 2020.
- [11] Z. Peng, T. Li, C. Pan, H. Ren, W. Xu, and M. D. Renzo, "Analysis and optimization for RIS-aided multi-pair communications relying on statistical CSI," *IEEE Trans. Veh. Technol.*, vol. 70, no. 4, pp. 3897–3901, Apr. 2021.
- [12] G. Zhou, C. Pan, H. Ren, K. Wang, and A. Nallanathan, "A framework of robust transmission design for IRS-aided MISO communications with imperfect cascaded channels," *IEEE Trans. Signal Process.*, vol. 68, pp. 5092–5106, Aug. 2020.
- [13] Q. Wu and R. Zhang, "Intelligent reflecting surface enhanced wireless network via joint active and passive beamforming," *IEEE Trans. Wireless Commun.*, vol. 18, no. 11, pp. 5394–5409, Aug. 2019.
- [14] C. Pan *et al.*, "Multicell MIMO communications relying on intelligent reflecting surfaces," *IEEE Trans. Wireless Commun.*, vol. 19, no. 8, pp. 5218–5233, Aug. 2020.
- [15] Z. Peng, Z. Zhang, C. Pan, L. Li, and A. L. Swindlehurst, "Multiuser full-duplex two-way communications via intelligent reflecting surface," *IEEE Trans. Signal Process.*, vol. 69, pp. 837–851, Jan. 2021.
- [16] T. Bai, C. Pan, Y. Deng, M. Elkashlan, A. Nallanathan, and L. Hanzo, "Latency minimization for intelligent reflecting surface aided mobile edge computing," *IEEE J. Sel. Areas Commun.*, vol. 38, no. 11, pp. 2666–2682, Nov. 2020.
- [17] C. Pan *et al.*, "Intelligent reflecting surface aided MIMO broadcasting for simultaneous wireless information and power transfer," *IEEE J. Sel. Areas Commun.*, vol. 38, no. 8, pp. 1719–1734, Jun. 2020.
- [18] T. Cui, S. Liu, and L. Zhang, "Information metamaterials and metasurfaces," *J. Phys. Chem. C*, vol. 5, no. 15, p. 3644–3668, Mar. 2017.
- [19] F. Liu *et al.*, "Intelligent metasurfaces with continuously tunable local surface impedance for multiple reconfigurable functions," *Phys. Rev. Appl.*, vol. 11, no. 4, p. 044024, Apr. 2019.
- [20] C. Pan *et al.*, "Reconfigurable intelligent surfaces for 6G systems: Principles, applications, and research directions," *IEEE Commun. Mag.*, vol. 59, no. 6, pp. 14–20, Jul. 2021.
- [21] C. You, Z. Kang, Y. Zeng, and R. Zhang, "Enabling Smart Reflection in Integrated Air-Ground Wireless Network: IRS Meets UAV," 2021. [Online]. Available: <https://arxiv.org/abs/2103.07151>
- [22] A. Sabri Abdalla, T. Faizur Rahman, and V. Marojevic, "UAVs with Reconfigurable Intelligent Surfaces: Applications, Challenges, and Opportunities," 2020. [Online]. Available: <https://arxiv.org/abs/2012.04775>
- [23] J. Ye, J. Qiao, A. Kammoun, and M.-S. Alouini, "Non-terrestrial Communications Assisted by Reconfigurable Intelligent Surfaces," 2021. [Online]. Available: <https://arxiv.org/abs/2109.00876>
- [24] A. Al-Hilo, M. Samir, M. Elhattab, C. Assi, and S. Sharafeddine, "RIS-Assisted UAV for Timely Data Collection in IoT Networks," 2021. [Online]. Available: <https://arxiv.org/abs/2103.17162>
- [25] A. Ranjha and G. Kaddoum, "URLLC facilitated by mobile UAV relay and RIS: A joint design of passive beamforming, blocklength, and UAV positioning," *IEEE Internet Things J.*, vol. 8, no. 6, pp. 4618–4627, Mar. 2021.
- [26] M. Hua, L. Yang, Q. Wu, C. Pan, C. Li, and A. Lee Swindlehurst, "UAV-assisted intelligent reflecting surface symbiotic radio system," *IEEE Trans. Wireless Commun.*, vol. 20, no. 9, pp. 5769–5785, Sep. 2021.
- [27] Z. Zhang, Q. Chang, N. Zhao, C. Li, and T. Li, "Data downlink system in the vast IOT node condition assisted by UAV, large intelligent surface, and power and data beacon," *Sensors*, vol. 20, p. 5748, 10 2020.
- [28] A. A. Khalil, M. Y. Selim, and M. A. Rahman, "CURE: Enabling RF energy harvesting using cell-free massive MIMO UAVs assisted by RIS," in *Proc. IEEE LCN*, Edmonton, AB, Canada, Oct. 2021, pp. 533–540.
- [29] K. Khac Nguyen, A. Masaracchia, T. Do-Duy, H. V. Poor, and T. Q. Duong, "RIS-assisted UAV communications for IoT with wireless power transfer using deep reinforcement learning," 2021. [Online]. Available: <https://arxiv.org/abs/2108.02889>
- [30] Z. Li, W. Chen, H. Cao, H. Tang, K. Wang, and J. Li, "Intelligent reflecting surface empowered UAV SWIPT networks," 2021. [Online]. Available: <https://arxiv.org/abs/2107.11016>
- [31] Y. Zeng, J. Xu, and R. Zhang, "Energy minimization for wireless communication with rotary-wing UAV," *IEEE Trans. Wireless Commun.*, vol. 18, no. 4, pp. 2329–2345, Apr. 2019.
- [32] T. Van Chien, H. Q. Ngo, S. Chatzinotas, M. Di Renzo, and B. Ottersten, "Reconfigurable intelligent surface-assisted cell-free massive MIMO systems over spatially-correlated channels," *IEEE Trans. Wireless Commun.*, early access, Dec. 2021, doi:[10.1109/TWC.2021.3136925](https://doi.org/10.1109/TWC.2021.3136925).
- [33] G. Zhou, C. Pan, H. Ren, K. Wang, and A. Nallanathan, "Intelligent reflecting surface aided multigroup multicast MISO communication systems," *IEEE Trans. Signal Process.*, vol. 68, pp. 3236–3251, 2020.
- [34] D. R. Hunter and K. Lange, "A tutorial on MM algorithms," *Am. Statist.*, vol. 58, no. 1, pp. 30–37, Feb. 2004.
- [35] Y. Sun, P. Babu, and D. P. Palomar, "Majorization-minimization algorithms in signal processing, communications, and machine learning," *IEEE Trans. Signal Process.*, vol. 65, no. 3, pp. 794–816, Feb. 2017.
- [36] S. Xu, "Smoothing method for minimax problems," *Comput. Optim. Appl.*, vol. 20, no. 3, pp. 267–279, Dec. 2001.
- [37] R. Varadhan and C. Roland, "Simple and globally convergent methods for accelerating the convergence of any EM algorithm," *Scand. J. Stat.*, vol. 35, no. 2, pp. 335–353, Jun. 2008.
- [38] A. Ben-Tal and A. Nemirovski, *Lectures on Modern Convex Optimization: Analysis, Algorithms, and Engineering Applications*. Philadelphia, PA, USA: SIAM, 2001.
- [39] "The MOSEK optimization toolbox for MATLAB manual," version 9.2 (revision 35). [Online]. Available: <http://mosek.com>, Accessed on: Jan. 2, 2021
- [40] X.-D. Zhang, *Matrix analysis and applications*. Beijing, CHN: Tsinghua Univ. Press, 2004.
- [41] H. Lütkepohl, *Handbook of matrices*. New York, NY, USA: Wiley, 1996.
- [42] J. R. Magnus and H. Neudecker, *Matrix differential calculus with applications in statistics and econometrics*. Hoboken, NJ, USA: Wiley, 1988.